
Non-hydrostatic Numerical Modeling of Hydraulic Jump over a Weir

Haiyang Cui

Graduation committee
Prof. Dr. Ir. G.S. Stelling
Dr.ir. M. Zijlema
Ir. T.J. Zitman

July 2, 2007
Delft University of Technology
Faculty of Civil Engineering and Geosciences
Section of Environmental Fluid Mechanics

Preface

This report is the Master of Science Thesis of Haiyang Cui, student from the Faculty of Civil Engineering at Delft University of Technology. In this master thesis several numerical studies are described on the hydraulic jump over a weir.

I would like to thank Prof. dr. ir. G.S. Stelling, for his daily supervision, continuous encouragement and valuable suggestions. I would also like to express my gratitude towards the other members of the graduation committee, Dr.ir. M. Zijlema, and Ir. T.J. Zitman. I thank my family for their support and understanding and my girlfriend, An Ran, for her love, support, and encouragement.

Haiyang Cui
Delft
July 2, 2007

Abstract

Weir is the construction widely used in hydraulic engineering. It is very important to investigate the behaviors of the flows over a weir. In general when water streams over a weir it behaves various flow patterns according to different flow conditions. Different flow patterns results in different inference on the water level profile and the distribution of recirculation zones at downstream of the weir. The simulation of these flows is of general practical interest to the design of hydraulic structures and the management of water resources.

In this report, a view of how to simulation hydraulic jump over a weir is presented, from 1-D model, 2DV hydrostatic model, 2DV non-hydrostatic model using pressure gradients as unknowns, 2DV non-hydrostatic model using pressures as unknowns, to 2DV implicit non-hydrostatic model.

In chapter 6, a 2DV implicit non-hydrostatic numerical scheme is presented, which can simulate flows with steep water and bed level gradients. The numerical algorithm solve the Reynolds equations and the integrated continuity equation simultaneously, so that the water surface level is integrated into the system, and solved together with the pressure fields. The resulting algorithm is locally and globally mass conservative. Several numerical experiments illustrate the potential of the model, namely: the simulation of the water level and velocity fields of free, undular and submerged hydraulic jumps downstream of a weir.

This model is proved to fairly accurately represent discontinuities in bottom topography and water surface profiles. The numerical model also has the ability to describe different flow regimes downstream of a weir, namely free flow, undulation, and fully submerged flow. The results from the numerical model show a fair agreement with the experimental data.

1D and hydrostatic modeling are not valid for the undulations behind an abrupt change in bottom profiles. The implicit non-hydrostatic model, provides the correct wave heights, wave lengths, and predict the upper and lower limit for the occurrence of undulations in a good manner.

Contents

1	Introduction	11
2	Numerical methods for rapidly varied flows in 1D	13
2.1	Shallow water equation in one-dimension	13
2.2	Numerical approximation of the equations	15
2.3	Numerical example of hydraulic jump simulation	18
3	Hydrostatic Two-dimensional vertical numerical model	21
3.1	Governing equations	21
3.2	Z-layers	23
3.3	Turbulence model	25
3.4	Numerical approximation	27
4	Non-hydrostatic 2DV model use pressure gradient as unknown	31
4.1	Model definitions	31
4.2	Governing equations	31
4.3	Discretisation of the equations	33
4.4	Solution of the system	34
4.5	Boundary conditions	37
4.6	Numerical examples	41
4.6.1	Standing wave in a closed basin	41
5	Implicit algorithm for Non-hydrostatic free-surface flow	45
5.1	Governing Equations	45
5.2	Numerical approximation	47
5.3	Sequence of the computation	48
5.4	Consideration of the bottom	50
5.5	Numerical examples	50
5.5.1	Oscillating basin	50
5.5.2	Hydraulic jump downstream of weir	51
5.5.3	Development of undulation downstream of a weir	53
5.5.4	The failure of the $k - \varepsilon$ model	64
5.6	Conclusions	67

6	Conclusions and Recommendations	69
6.1	Conclusions	69
6.2	Recommendations	70
A	Double sweep method for tridiagonal systems	73
B	Discretization of Advection terms	75
C	Comparison between Compact and Keller-box method	77

List of Figures

2.1	Flow schematisation	14
2.2	1D Staggered grid	16
2.3	Schematisation of conservation properties for weir flow with a hydraulic jump	17
2.4	Hydraulic jump, with momentum balance or energy head balance, depending on local flow conditions,(a) smooth bed (b)rough bed with Chezy number $C = 60m^{1/2}/s$	19
2.5	Hydraulic jump, with energy head balance at each grid point,(a) smooth bed (b)rough bed with Chezy number $C = 60m^{1/2}/s$	19
2.6	Hydraulic jump, with momentum balance at each grid point,(a) smooth bed (b)rough bed with Chezy number $C = 60m^{1/2}/s$	19
3.1	The velocities along the column are identical with smooth bed	24
3.2	The schematisation of back tracking method	25
3.3	The schematisation of the programming trick	26
3.4	Arrangement of the unknowns in a staggered grid	27
3.5	2D model without viscosity, smooth bed	29
3.6	2D model without viscosity, smooth bed,horizontal velocity distribution	30
3.7	2D model without viscosity, smooth bed,horizontal velocity vector distribution	30
4.1	Definition sketch of a classic staggered grid (a) and the stag- gered grid for the new approach (b).	32
4.2	Cell definition sketch of the staggered grid	32
4.3	The 4D matrix indicates the relation of the equation m,k with its neighbours	34
4.4	The horizontal momentum equation is coupled to all vertical pressure gradients towards the water surface	36
4.5	38
4.6	38
4.7	Open velocity boundary	39
4.8	Open water level boundary	40

4.9	Geometry of the basin	41
4.10	Water levels at location $x=10m$ of the standing wave in the closed basin. Comparison with hydrostatic and non-hydrostatic. $\Delta t = 0.01s$	42
4.11	Water level at station $x = 10m$ of the standing wave in closed basin. Comparison of the results of 1 layer and 2 layers.	43
4.12	Geometry of the basin	43
4.13	Water levels at location $x=10m$ of the standing wave in the closed basin. $\Delta t = 0.01s$	44
5.1	The structure of the coefficients and unknowns of the implicit approach.	46
5.2	The structure of the coefficients and unknowns of the implicit approach.	49
5.3	Bottom cell schema.	51
5.4	Water levels at locations $x=10m$ of the standing wave in the closed basin. $\theta=0.0$, compact method	52
5.5	Velocity vectors, at time $t = T/4$, with the non-hydrostatic pressure approximation.	52
5.6	Simulation of the oscillating basin with large Courant number, (a) Courant number=2.0 (b) Courant number=20.	53
5.7	Water level	54
5.8	Velocity vectors in front of the weir	55
5.9	Velocity vectors behind the weir	56
5.10	Flow regimes over a weir, type of flow regime depends on the degree of submergence.	57
5.11	The water profiles of all the conducted numerical experiments	60
5.12	Bottom profile.	61
5.13	Definition of the variables concerning the undulations behind a weir.	62
5.15	The comparison of the water profiles of numerical model with experiments data	63
5.16	Velocity vectors behind the weir, $Q=30[l/s]$	64
5.17	Comparison of velocity profile at different cross-sections, $Q=30$	66
5.18	The comparison of the water profiles of numerical model with experiments data, $Q=30[l/s]$, using $k - \varepsilon$ model.	66
5.19	Velocity vectors behind the weir, $Q=30[l/s]$., using $k - \varepsilon$ model.	67
C.1	The Keller-box method and Compact method	78

Chapter 1

Introduction

Phenomena like bores due to dam break, tidal bores, and hydraulic jump are all examples of rapidly varied free surface flows. In most cases these flows are simulated with hydrostatic models which are widely used in studying shallow rivers, lakes and estuaries. The hydrostatic pressure assumption is valid in most cases. However, there are also many cases where this assumption may be questionable. One example is the flow over a weir with a hydraulic jump. Modeling this kind of rapidly varied flow requires more sophisticated models. These models have to account for the effect of the non-hydrostatic pressure.

In order to account for the effect of vertical acceleration of fluids, the full Navier-Stokes equations must be solved. Harlow and Welch [4] are the first one who developed such kind of model by using the Marker-and-Cell (MAC) method. With the rapid increase in computer power in recent years, three dimensional hydrodynamic models are increasingly being developed for such free-surface flow problems. Various papers have been published on direct numerical simulation of non-hydrostatic flows. Stansby and Zhou (1998) [8] developed a two-dimensional vertical flow model for simulating the non-hydrostatic problem in sigma coordinates based on a pressure correction method. Casulli and Stelling (1998) [2] developed a three-dimensional quasi-hydrostatic model, in which the pressure decomposed into the sum of hydrostatic component and a hydrodynamic component. Zijlema (2000) [15] reported the extension of TRIWAQ (Rijkwaterstaat) with the effect of the non-hydrostatic pressure, using a pressure correction method. Stelling and Van Kester (2000) [10] present a new vertical approximation based on a Hermitian method.

Recently, Stelling and Zijlema (2003) [11] proposed a Keller-box scheme that specifies unknown pressure components at the cell surfaces of the vertical grids, rather than at the cell center. An exact zero pressure condition at the free surface thereby can be imposed. Their model with only two vertical layers is capable of predicting accurate free surface waves.

In the present report, a 2DV implicit non-hydrostatic numerical scheme

based on Stelling and Zijlema's method is presented. The numerical algorithm solves the Reynolds equations and the integrated continuity equation simultaneously, so that the water surface level can be integrated into the system, and solved together with the pressure field. The resulting algorithm is locally and globally mass conservative.

Chapter 2 describes the numerical scheme in 1D. The importance of conservation of properties in dealing with discontinuities is shown by compare of results with different momentum discretizations.

Chapter 3 presents the two-dimensional vertical numerical approximation of Reynolds averaged Navier-Stokes equations with hydrostatic assumption. A requirement for hydrostatic model under z -coordinate is proposed.

Chapter 4 and 5 describe the 2DV non-hydrostatic model, which use pressure gradients and pressures and unknowns respectively.

Chapter 6 describes the extension of 2DV non-hydrostatic model presented in Chapter 5. The final model couple the water level to the solution system implicitly. The application of the numerical model to simulate the hydraulic jump and undulations behind a weir is presented. In this chapter, the ability of the numerical model to represent the transition from fully submerged flow to hydraulic jump, to undulation, then to free flow is illustrated as well.

Chapter 7 gives general conclusion on the application of the numerical model. The existing problems and suggestions on further improvement is included.

Chapter 2

Numerical methods for rapidly varied flows in 1D

Rapidly varied flows occur, for instance, in hydraulic jumps and bores. Most numerical methods that can include these phenomenons are based upon explicit schemes and non-staggered grids, such as the Godunov methods. In this work, the numerical technique proposed by Stelling et al. (2003) [12] which is based upon classical staggered grids and implicit integration schemes is applied, which can combine the efficiency of staggered grids with conservation properties so as to ensure accurate results for rapidly varied flows, as well in expansions as in contractions. The shallow water equations are approximated so that proper mass and momentum balances are fulfilled.

2.1 Shallow water equation in one-dimension

The one-dimensional shallow-water equations in non-conservative form, are given by

$$\frac{\partial \zeta}{\partial t} + \frac{\partial(hu)}{\partial x} = 0 \quad (2.1)$$

$$\frac{\partial u}{\partial t} + u \frac{\partial u}{\partial x} + g \frac{\partial \zeta}{\partial x} + c_f \frac{u|u|}{h} = 0 \quad (2.2)$$

where(see Figure (2.1))

- u = depth-averaged velocity
- d = bottom depth below reference level
- ζ = water level above reference level
- h = $\zeta+d$ total water depth
- g = gravitational acceleration
- c_f = dimensionless bottom friction coefficient

The physical domain is depicted in Figure (2.1). The free surface is represented by the function ζ at position x and time t , which is the distance between the surface and the level of reference. This function is called the

water level. The bottom is described by the function $d(x)$, which gives the time-independent depth below the level of reference. The function $h(x, t) = \zeta(x, t) + d(x)$ is called the total water depth.

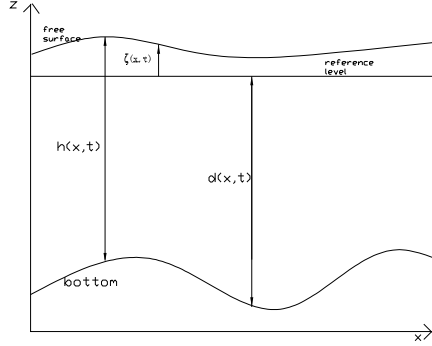


Figure 2.1: Flow schematisation

If the bottom is supposed not to be time varying, we have the following relations:

$$\frac{\partial \zeta}{\partial t} = \frac{\partial h}{\partial t} \quad (2.3)$$

The advection term can also be denoted with the following identities:

$$u \frac{\partial u}{\partial x} = \frac{1}{h} \left(\frac{\partial(hu^2)}{\partial x} - u \frac{\partial(hu)}{\partial x} \right) = \frac{1}{h} \left(\frac{\partial(qu)}{\partial x} - u \frac{\partial q}{\partial x} \right)$$

$$u \frac{\partial u}{\partial x} = \frac{\partial}{\partial x} \left(\frac{1}{2} u^2 \right)$$

with $q = uh$.

The flux formulation

The flux formulation of the shallow water equations in one dimensional reads:

$$\frac{\partial U}{\partial t} + \frac{\partial F(U)}{\partial x} = N(U) \quad (2.4)$$

where:

$U(x, t)$ = the vector conserved variables

$F(U)$ = the vector of fluxes

$N(U)$ = the vector of non-homogeneous terms

They are defined as:

$$U = \begin{pmatrix} h \\ q \end{pmatrix} \quad (2.5)$$

$$F(U) = \begin{pmatrix} q_l \\ q_l^2/h + \frac{1}{2}gh^2 \end{pmatrix} \quad (2.6)$$

$$N(U) = \begin{pmatrix} 0 \\ gh \frac{\partial d}{\partial x} \end{pmatrix} \quad (2.7)$$

where the conserved variables are the total water depth h and the discharge per unit width $q_l = uh$. The flux term $1/2gh^2$ and the non-homogeneous term $gh\partial d/\partial x$ arise from splitting the hydrostatic pressure term $p = g(\zeta - z)$, into a gradient of the water depth and the bottom slope as follows:

$$gh \frac{\partial \zeta}{\partial x} = gh \frac{\partial}{\partial x}(h - d) = \frac{\partial}{\partial x} \left(\frac{1}{2}gh^2 \right) - gh \frac{\partial d}{\partial x} \quad (2.8)$$

This formulation is just derived from mathematical manipulation and does not necessarily represent a proper momentum balance. In the case of discontinuous steps in the bottom profile, the term $\partial d/\partial x$ might tend to infinity.

2.2 Numerical approximation of the equations

At local discontinuities Equations (2.1) and (2.2) have no unique solution. Rapidly varied flows are typically non-hydrostatic, they would require 3D non-hydrostatic free surface flow approximations. However, using law of conservation, it is sufficient to get solutions of local energy losses, location of a hydraulic jump, propagation speed of a bore, etc. The numerical technique proposed by Stelling et al.(2003) [12] which is based upon classical staggered grids and implicit numerical integration schemes is applied, which can be applied to problems that includes rapidly varied flows.

Approximation of the continuity equation

A common grid for the approximation of equations is a staggered grid as given in Figure 2.2. By using Eq.(2.3), Eq.(2.1) can be written as:

$$\frac{\partial h}{\partial t} + \frac{\partial(hu)}{\partial x} = 0 \quad (2.9)$$

A simple discretization of Equation(2.9) is given by:

$$\frac{h_i^{n+1} - h_i^n}{\Delta t} + \frac{{}^*h_{i+1/2}^n u_{i+1/2}^{n+\theta} - {}^*h_{i-1/2}^n u_{i-1/2}^{n+\theta}}{\Delta x} = 0 \quad (2.10)$$

In the staggered grid, the values of *h at points numbered by $(i+1/2)$ are missing. These missing values are approximated by first-order upwinding as follows:

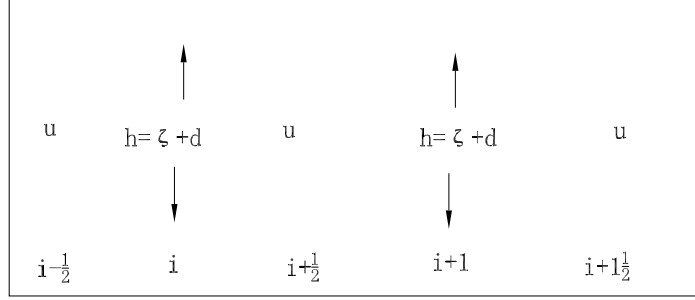


Figure 2.2: 1D Staggered grid

$${}^*h_{i+1/2} = \begin{cases} h_i, & \text{if } u_{i+1/2} > 0 \\ h_{i+1}, & \text{if } u_{i+1/2} < 0 \\ \max(\zeta_i, \zeta_{i+1}) + \min(d_i, d_{i+1}), & \text{if } u_{i+1/2} = 0 \end{cases}$$

To derive conditions for non-negative solutions for water depth, we rewrite eq. (2.10), while we assume positive flows, as:

$$h_i^{n+1} = \left(1 - \frac{\Delta t u_{i+1/2}^{n+\theta}}{\Delta x}\right) h_i^n + \frac{\Delta t u_{i-1/2}^{n+\theta}}{\Delta x} h_{i-1}^n, \quad u_{i+1/2}^{n+\theta} \geq 0, u_{i-1/2}^{n+\theta} \geq 0 \quad (2.11)$$

From this it follows that strict positivity of the water depth is ensured if:

$$\frac{\Delta t u_{i+1/2}^{n+\theta}}{\Delta x} < 1 \quad (2.12)$$

Similar approach can be done for the negative flow direction. Simply fulfilling eq.(2.12) will prevent wet points from drying. So no special drying and flooding procedures are required.

Approximation of the momentum equation

The momentum equation is discretized as follows:

$$\frac{u_{i+1/2}^{n+1} - u_{i+1/2}^n}{\Delta t} + ADV(u_i^{n+1}, u_{i+1/2}^n) + g \frac{\zeta_{i+1}^{n+1} - \zeta_i^{n+1}}{\Delta x} + c_f \frac{|u_{i+1/2}^n| u_{i+1/2}^{n+1}}{\bar{h}_{i+1/2}^n} = 0 \quad (2.13)$$

where $\bar{h} = \frac{h_i + h_{i+1}}{2}$, ADV stands for an approximation of advection term.

To get accurate results for rapidly varied flows, conservation of properties become crucial. In flow expansions, a numerical approximation is applied that ensures momentum balance, while in strong contractions, energy head conservation approximation is applied (see Figure 2.3). So the discretization of the advection term is treated in two different ways.

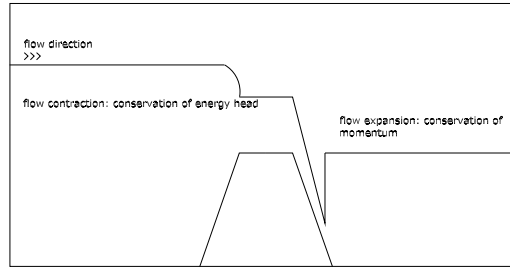


Figure 2.3: Schematisation of conservation properties for weir flow with a hydraulic jump

$$u \frac{\partial u}{\partial x} \approx \frac{\bar{q}_i}{\bar{h}_{i+1/2}} \left(\frac{u_{i+1/2} - u_{i-1/2}}{\Delta x} \right) = \frac{1}{\bar{h}_{i+1/2}} \left(\frac{\bar{q}_{i+1} u_{i+1/2} - \bar{q}_i u_{i-1/2}}{\Delta x} - u_{i+1/2} \frac{\bar{q}_{i+1} - \bar{q}_i}{\Delta x} \right) \quad (2.14)$$

$$u \frac{\partial u}{\partial x} \approx \frac{1}{2} (u_{i+1/2} + u_{i-1/2}) \left(\frac{u_{i+1/2} - u_{i-1/2}}{\Delta x} \right) = \frac{1/2 u_{i+1/2}^2 - 1/2 u_{i-1/2}^2}{\Delta x} \quad (2.15)$$

If $\frac{u_{i+1/2} - u_{i-1/2}}{\Delta x} > \varepsilon > 0$, then use Equation (2.15) else use Equation (2.14).

To improve the numerical accuracy, the missing values of u at points numbered by (i) are approximated by second-order upwinding extrapolation in

combination with *slope limiters*, similar to the *flux limiters* as described by Hirsch [5].

For positive flow direction the extrapolations are given by:

$${}^*u_i = u_{i-1/2} + \frac{1}{2}\Psi(r_u)(u_{i-1/2} - u_{i-3/2})$$

Here for the slope limiter we use *Van Leer limiter*, which is given by:

$$\text{Van Leer: } \Psi(r) = \frac{r + |r|}{1 + r}$$

where r is given by: $r = \frac{\zeta_{i+1} - \zeta_i}{\zeta_i - \zeta_{i-1}}$.

The system of equations is solved by substituting the velocities at the new time step $n + 1$ obtained from (2.13) into equation (2.10). The resulting equation constitutes a tri-diagonal system with water levels as unknowns. The system is solved by applying the double sweep algorithm (see Appendix A). Once the water levels have been computed the new velocities are obtained directly from equation (2.13). Boundary conditions are defined upstream and downstream, which specify discharge or velocity and water level respectively.

2.3 Numerical example of hydraulic jump simulation

The steady state flow over a triangular weir is simulated. The length of the channel is $L=100\text{m}$, unitary width $B=1\text{m}$, and the bottom topography is defined as:

$$d(x) = \begin{cases} 10.0 - (x - 40) * 8.0/10, & \text{if } 40\text{m} \leq x \leq 50\text{m} \\ 2.0 + (x - 50) * 8.0/10, & \text{if } 50\text{m} \leq x \leq 60\text{m} \\ 10.0, & \text{otherwise} \end{cases}$$

At inflow a discharge equals to $10.0\text{m}^3/\text{s}$ is prescribed and at outflow a water depth of -2.0m is imposed.

Figures 2.4 to 2.6 show the results taking $\Delta x = 0.1\text{m}$ and $\Delta t = 0.005\text{s}$.

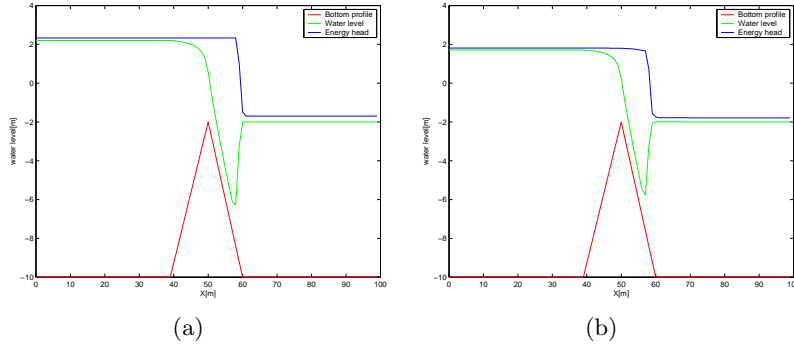


Figure 2.4: Hydraulic jump, with momentum balance or energy head balance, depending on local flow conditions,(a) smooth bed (b)rough bed with Chezy number $C = 60m^{1/2}/s$.

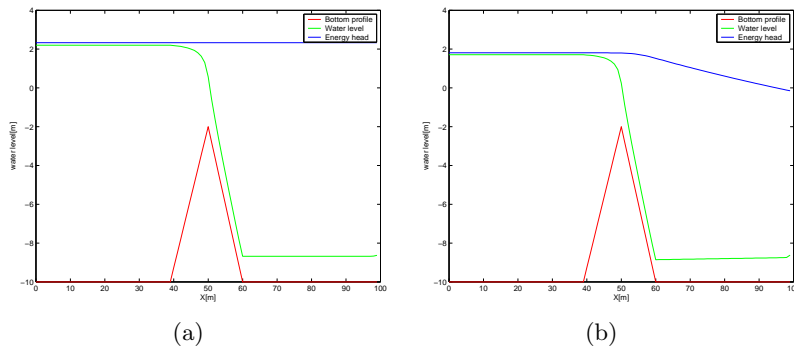


Figure 2.5: Hydraulic jump, with energy head balance at each grid point,(a) smooth bed (b)rough bed with Chezy number $C = 60m^{1/2}/s$.

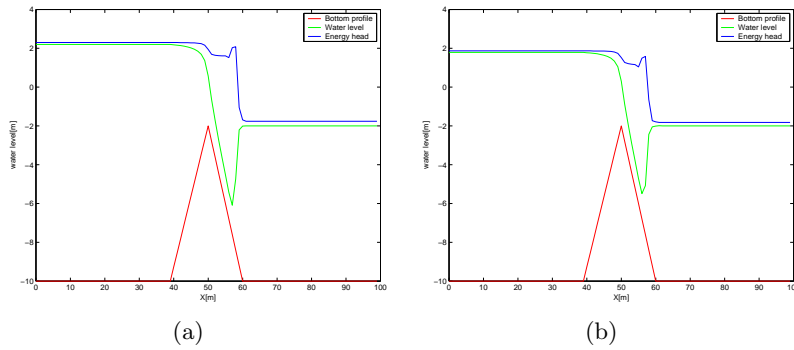


Figure 2.6: Hydraulic jump, with momentum balance at each grid point,(a) smooth bed (b)rough bed with Chezy number $C = 60m^{1/2}/s$.

Chapter 3

Hydrostatic Two-dimensional vertical numerical model

3.1 Governing equations

The governing equations are the Reynolds-averaged Navier-Stokes equations for incompressible fluid.

Momentum Equations:

$$\frac{\partial u}{\partial t} + u \frac{\partial u}{\partial x} + w \frac{\partial u}{\partial z} = -\frac{\partial p}{\partial x} + v^h \frac{\partial^2 u}{\partial x^2} + \frac{\partial}{\partial z} \left(v^v \frac{\partial u}{\partial z} \right) \quad (3.1)$$

$$\frac{\partial w}{\partial t} + u \frac{\partial w}{\partial x} + w \frac{\partial w}{\partial z} = -\frac{\partial p}{\partial z} + v^h \frac{\partial^2 w}{\partial x^2} + \frac{\partial}{\partial z} \left(v^v \frac{\partial w}{\partial z} \right) - g \quad (3.2)$$

Continuity equation:

$$\frac{\partial u}{\partial x} + \frac{\partial w}{\partial z} = 0 \quad (3.3)$$

where

u = velocity components in the horizontal x direction

w = velocity components in the horizontal z direction

t = time

p = normalised pressure defined as the pressure divided by a constant reference density

g = gravitational acceleration

v^h = horizontal viscosity

v^v = vertical viscosity

The Shallow Water Approximation

$$\underbrace{\frac{\partial u}{\partial x}}_{\frac{U}{L}} + \underbrace{\frac{\partial w}{\partial z}}_{\frac{W}{D}} = 0 \quad (3.4)$$

If the horizontal length scale of motion L is much greater than the water depth D , i.e., shallow water,

$$\frac{D}{L} \ll 1 \quad (3.5)$$

we have

$$W = \frac{DU}{L} \ll U \quad (3.6)$$

Under these conditions, the Reynolds-averaged Navier-Stokers equations may be reduced to the boundary layer form. The momentum in z direction then reduces to the hydrostatic pressure assumption:

$$\frac{\partial p}{\partial z} = -\rho g \quad (3.7)$$

The vertical velocity w is determined by continuity only. The momentum equaiton reduces to:

$$\frac{\partial u}{\partial t} + u \frac{\partial u}{\partial x} + w \frac{\partial u}{\partial z} = -g \frac{\partial \zeta}{\partial x} + v^h \frac{\partial^2 u}{\partial x^2} + \frac{\partial}{\partial z} \left(v^v \frac{\partial u}{\partial z} \right) \quad (3.8)$$

$$\frac{\partial w}{\partial t} + u \frac{\partial w}{\partial x} + w \frac{\partial w}{\partial z} = v^h \frac{\partial^2 w}{\partial x^2} + \frac{\partial}{\partial z} \left(v^v \frac{\partial w}{\partial z} \right) \quad (3.9)$$

Boundary conditions:

The boundary conditions at the free surface($z=\zeta$) and at the bottom($z=-d$) read:

Kinematic conditions:

$$w|_{z=\zeta} = \frac{\partial \zeta}{\partial t} + u \frac{\partial \zeta}{\partial x} \quad (3.10)$$

$$w|_{z=-d} = -u \frac{\partial d}{\partial x}$$

By means of integration of the continuity equation (3.1) over the depth $H = \zeta + d$, and subsequent the use of of the Leibniz's rule and insertion to the kinematic conditions, gives:

$$\frac{\partial \zeta}{\partial t} + \frac{\partial}{\partial x} \left[\int_{-d}^{\zeta} u dz \right] = 0 \quad (3.11)$$

At the bed, the bottom shear stress is prescribed as $v^v \frac{\partial u}{\partial z} = \frac{\tau_b}{\rho}$. The bottom shear stress τ_b is defined as $\tau_b = \rho u_*^2$, where the bed shear velocity can be obtained from the assumption of logarithmic law of the wall:

$$u(z) = \frac{u_*}{\kappa} \ln \left(\frac{z + z_0}{z_0} \right) \quad (3.12)$$

where: κ is the Von Karman constant and z_0 is the friction parameter.

3.2 Z-layers

This approach is formulated in the Cartesian co-ordinates. The horizontal index for the grid points is denoted by m , the vertical index for the grid is denoted by k . The indices m and k increase as x and z increases. Because the free surface varies as a function of time, the number of active grid layers may be function of time and space. We introduce a set of vertical levels

$$\{z_{k-1/2} | k = 1, \dots, K + 1 \wedge \forall(x, y) : z_{1/2} \leq -d(x, y) \leq \zeta(x, y, t) \leq z_{K+1/2}\} \quad (3.13)$$

A cell with centre at (x_i, z_k) is bounded by the intersection of the water column with the horizontal levels $z_{k\pm 1/2}$ and the horizontal grid lines $x_{k\pm 1/2}$. The strictly horizontal layers cause the number of layers to vary as a function of the depth as well as the surface elevation. Therefore the layer thickness at the surface and at the bottom will be different from the thickness in between. The layer thickness of the cell is defined as:

$$\Delta z_k^n = \min[\zeta_{i, z_{k+1/2}}, z_{K+1/2}] - \max[-d_i, z_{K-1/2}] \quad (3.14)$$

with n denoting the present time level. A cell is wet as long as $\Delta z_k^n > 0$, which means the control volumes are occupied by fluid. Due to the variation of the free surface, the number of wet cells in the water column change along time. So indices are needed to indicate the position of the free surface and bottom. The vertical index of the cell at free surface is denoted as $k_{top}(i)$, whereas the cell just above the bottom is denoted as $k_{bottom}(i)$.

Note that at the u points the layer thickness is not uniquely defined. Here we implement an upwind approach, which means that the layer thickness is determined by the direction of the flow. For this purpose the operator mu is used, which is defined by:

$$mu(m) = \begin{cases} m & \text{if } u_m > 0 \\ m + 1 & \text{if } u_m < 0 \\ m & \text{if } u_m = 0 \wedge \zeta_m > \zeta_{m+1} \\ m + 1 & \text{if } u_m = 0 \wedge \zeta_m < \zeta_{m+1} \end{cases} \quad (3.15)$$

A requirement for schemes using fixed layers

In 2D vertical or 3D computational modeling of fluid dynamics, if the bottom is smooth and the viscosity is not taken into account, any scheme for advection should give identical results as 1D model at the same location, while the horizontal velocities along the vertical column should be the same (see figure(3.1)).

We demonstrate this requirement by an example. For the velocity $u(i, j)$,

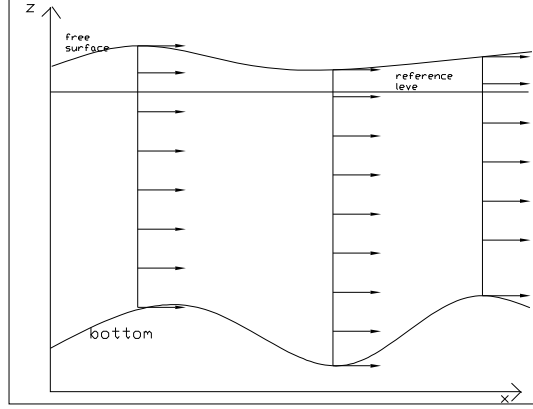


Figure 3.1: The velocities along the column are identical with smooth bed

the discharge below this point is denoted as $q(i, j)$. At location $(i - 1)$, we find out such a point where $q(i - 1, j_{mark}) = q(i, k)$. The velocity at that point is denoted as u_{back} . If there is no such point in the coordination, interpolation is used to get it. Below these two points, the discharge are the same, then the line along these two points can be considered as a streamline.

$$\begin{aligned}
 u(i, j) \frac{(u(i, j) - u_{back})}{\Delta x} &= u(x, z) \frac{u(x, z) - u(x - \Delta x, z - \Delta z)}{\Delta x} + \\
 &= u(x, z) \frac{u(x, z) - (u(x, z) - \Delta x u_x - \Delta z u_z + \frac{1}{2}(\Delta x^2 u_{xx} + 2\Delta x \Delta z u_{xz} + \Delta z^2 u_{zz}) + \dots)}{\Delta x} \\
 &= u(x, z) \frac{\Delta x u_x + \Delta z u_z - \frac{1}{2}(\Delta x^2 u_{xx} + 2\Delta x \Delta z u_{xz} + \Delta z^2 u_{zz}) + \dots}{\Delta x} \\
 &= u u_x + u \frac{\Delta z}{\Delta x} u_z - \frac{1}{2} u (\Delta x u_{xx} + 2\Delta z u_{xz} + \frac{\Delta z^2}{\Delta x} u_{zz}) \\
 &= u u_x + u \frac{\Delta z}{\Delta x} u_z + error
 \end{aligned} \tag{3.16}$$

If AB is a streamline, then $|AC|w = u|BC|$, i.e. $\Delta x w = \Delta z u$, $w = \Delta z u / \Delta x$, which means:

$$u(i, j) \frac{(u(i, j) - u_{back})}{\Delta x} = u u_x + u \frac{\Delta z}{\Delta x} u_z + error = u u_x + w u_z + error \tag{3.17}$$

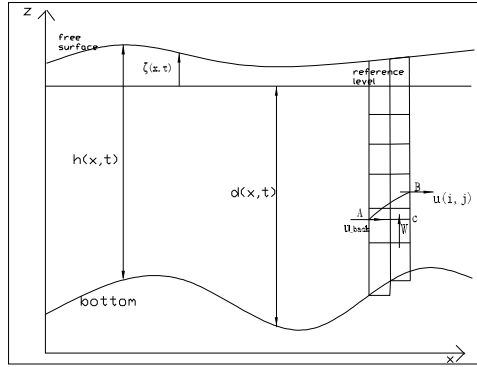


Figure 3.2: The schematisation of back tracking method

Based on the theoretical analysis, the method of back tracking can take both horizontal and vertical advection into account. However, in practice, when the boundary is non-reflective, this method can work well. If the downstream boundary is reflective, this method will not fulfill the requirement mentioned above.

A trick in programming under cartesian coordination

In programming, the velocity above the free surface should be set to equal the one at the free surface. Otherwise, when the free surface changes, in next computation step, the velocity used at the new wet cells is zero (initial value) other than the old velocity at the old free surface. This will introduce disturbance and make the computation less convergent. (See figure (3.3))

3.3 Turbulence model

The turbulence model implemented is the standard $k - \varepsilon$ model (Rodi 1980) [7].

$$\frac{\partial k}{\partial t} + \frac{\partial uk}{\partial x} + \frac{\partial wk}{\partial z} = \frac{\partial}{\partial x} \left[\frac{v^v}{\sigma_k} \frac{\partial k}{\partial x} \right] + \frac{\partial}{\partial z} \left[\frac{v^v}{\sigma_k} \frac{\partial k}{\partial z} \right] + P_k - \varepsilon \quad (3.18)$$

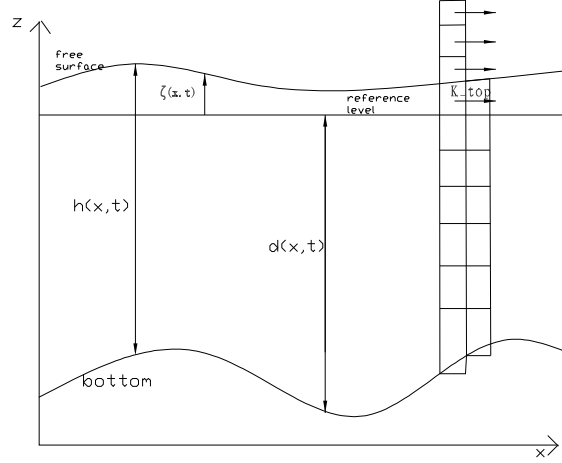


Figure 3.3: The schematisation of the programming trick

$$\frac{\partial \varepsilon}{\partial t} + \frac{\partial u \varepsilon}{\partial x} + \frac{\partial w \varepsilon}{\partial z} = \frac{\partial}{\partial x} \left[\frac{v^v}{\sigma_\varepsilon} \frac{\partial \varepsilon}{\partial x} \right] + \frac{\partial}{\partial z} \left[\frac{v^v}{\sigma_\varepsilon} \frac{\partial \varepsilon}{\partial z} \right] + \frac{\varepsilon}{k} [c_{1\varepsilon} P_k - c_{2\varepsilon} \varepsilon] \quad (3.19)$$

where:

$$P_k = 2v^v \left(\frac{\partial u}{\partial x} \right)^2 + 2v^v \left(\frac{\partial w}{\partial z} \right)^2 + v^v \left(\frac{\partial u}{\partial x} + \frac{\partial w}{\partial z} \right)^2 \quad (3.20)$$

where v^v is the eddy viscosity, k is the turbulent kinetic energy and ε is the dissipation rate of the turbulent kinetic energy.

The eddy viscosity is related to k by:

$$v^v = c_\mu \frac{k^2}{\varepsilon} \quad (3.21)$$

The empirical constants are given as:

$$c_\mu = 0.09, c_{1\varepsilon} = 1.44, c_{2\varepsilon} = 1.92, \sigma_k = 1.0, \sigma_\varepsilon = 1.3 \quad (3.22)$$

The boundary conditions are given by:

At surface:

$$\begin{aligned} k &= 0 \\ \varepsilon &= 0 \end{aligned} \quad (3.23)$$

At the bottom:

$$\begin{aligned} k &= \frac{1}{\sqrt{c_\mu}} u_*^2 \\ \varepsilon &= \frac{u_*^2}{\kappa z_0} \end{aligned} \quad (3.24)$$

where: κ is the Von Karman constant and z_0 is the friction parameter. Generally, $\kappa = 0.41, z_0 = 0.000025m$.

The above model is only appropriate for modeling high-Reynolds number flow regions. If flows with solid boundaries are to be calculated, the model has to be in conjunction with empirical laws that connect the wall conditions (e.g. bottom shear stress) to the dependent variables outside the viscous sublayer.

3.4 Numerical approximation

For the numerical application a fully staggered grid, so-called C grid, is applied. Water level is approximated at locations (i,k) , while horizontal velocities at $(i+1/2,k)$ and vertical velocities at $(i,k+1/2)$ (See Figure 3.4). The staggered grid has many advantages (Stelling, 1984) [9]. First, it can reduce the computational values. Secondly, it makes the implementation of boundary conditions simple. At last, the staggered grid excludes spurious oscillations.

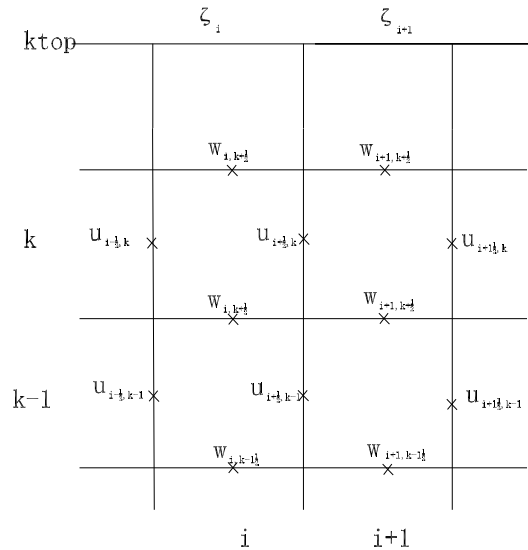


Figure 3.4: Arrangement of the unknowns in a staggered grid

An explicit discretization for the momentum equations takes the following

form:

$$u_{i+1/2,k}^{n+1} = u_{i+1/2,k}^n - \Delta t ADV(u_{i+1/2,k}^n, u_{i+1/2,k}^{n+1}) + \Delta t HV(u_{i+1/2,k}^n) + \Delta t VV(u_{i+1/2,k}^{n+1}) - g \frac{\Delta t}{\Delta x} (\zeta_{i+1}^n - \zeta_i^n) \quad (3.25)$$

in which VV and HV stand for approximation for the vertical viscosity and horizontal viscosity respectively. The equation (3.25) forms a linear tri-diagonal system with unknowns u^{n+1} in the same water column. The horizontal velocity can be obtained by the double sweep algorithm. After that, the discharge at each water column can be obtained by

$$q_i^n = \sum_{k=k_{bottom}}^{k_{top}} u(i, k) dz(i, k)$$

Then the water level ζ and vertical velocity w can be obtained by global and local mass conservation respectively.

$$\zeta_i^{n+1} = \zeta_i^n - \frac{\Delta t}{\Delta x} (q_i^n - q_{i-1}^n) \quad (3.26)$$

$$w_{i,k}^{n+1} = w_{i,k-1}^n - \frac{\Delta z_{m,k}}{\Delta x} (u_{i,k}^{n+1} - u_{i-1,k}^{n+1}) \quad (3.27)$$

Advection and viscosity approximations

The horizontal advection term is approximated as follows:

$$ADV(u_{i+1/2,k}^n, u_{i+1/2,k}^{n+1}) = \frac{1}{2} (u_{i+1/2,k}^n + u_{i-1/2,k}^n) \left(\frac{u_{i+1/2,k}^n - u_{i-1/2,k}^n}{\Delta x} \right) \quad (3.28)$$

$$ADV(u_{i+1/2,k}^n, u_{i+1/2,k}^{n+1}) = \begin{cases} u_{i+1/2,k} \left(\frac{u_{i+1/2,k}^n - u_{i-1/2,k}^n}{\Delta x} \right) & \text{when } u_{i+1/2,k}^n > u_{i-1/2,k}^n \\ u_{i+1/2,k} \left(\frac{u_{i+3/2,k}^n - u_{i+1/2,k}^n}{\Delta x} \right) & \text{when } u_{i+1/2,k}^n \leq u_{i-1/2,k}^n \end{cases} \quad (3.29)$$

If $\frac{u_{i+1/2}^n - u_{i-1/2}^n}{\Delta x} > \varepsilon > 0$, then use Equation (3.28) else use Equation (3.29).

The vertical advection term is approximated as follows:

$$ADV(w_{i,k+1/2}^n) = \begin{cases} \bar{w}_- \left(\frac{u_{i+1/2}^n - u_{i-1/2}^n}{\Delta z} \right) & \text{when } \bar{w}_+ > 0 \cap \bar{w}_- > 0 \\ \bar{w}_+ \left(\frac{u_{i+1/2}^n - u_{i-1/2}^n}{\Delta z} \right) & \text{when } \bar{w}_+ < 0 \cap \bar{w}_- < 0 \\ \bar{w}_+ \left(\frac{u_{i+1/2}^n - u_{i-1/2}^n}{\Delta z} \right) + \bar{w}_- \left(\frac{u_{i+1/2}^n - u_{i-1/2}^n}{\Delta z} \right) & \text{when } \bar{w}_+ < 0 \cap \bar{w}_- > 0 \end{cases} \quad (3.30)$$

where:

$$\begin{aligned}
\bar{w}_+ &= \frac{w_{i,k+1/2} + w_{i,k+3/2}}{2} \\
\bar{w}_- &= \frac{w_{i,k+1/2} + w_{i,k-1/2}}{2} \\
u_{,-1} &= u_{i+1/2,k-1} \\
u_{,+1} &= u_{i+1/2,k+1}
\end{aligned} \tag{3.31}$$

The horizontal viscosity is approximated by:

$$HV(u_{i+1/2,k}^n) = \frac{v_{i+1/2,k}^{hn}}{\Delta x} \left(\left(\frac{u_{i+1,k} - u_{i,k}}{\Delta x} \right) - \left(\frac{u_{i,k} - u_{i-1,k}}{\Delta x} \right) \right) \tag{3.32}$$

The vertical viscosity is approximated by:

$$VV(u_{i+1/2,k}^{n+1}) = \frac{v_{i+1/2,k+1/2}^{vn} \frac{u_{i+1/2,k+1}^{n+1} - u_{i+1/2,k}^{n+1}}{\Delta z_{i+1/2,k+1/2}^n} - v_{i+1/2,k-1/2}^{vn} \frac{u_{i+1/2,k}^{n+1} - u_{i+1/2,k-1}^{n+1}}{\Delta z_{i+1/2,k-1/2}^n}}{\Delta z_{i+1/2,k}^n} \tag{3.33}$$

Figure 3.5 shows the results taking $\Delta x = 0.5m$ and $\Delta t = 0.01s$. The small difference between that of 1D model is due to the large space step. Figure

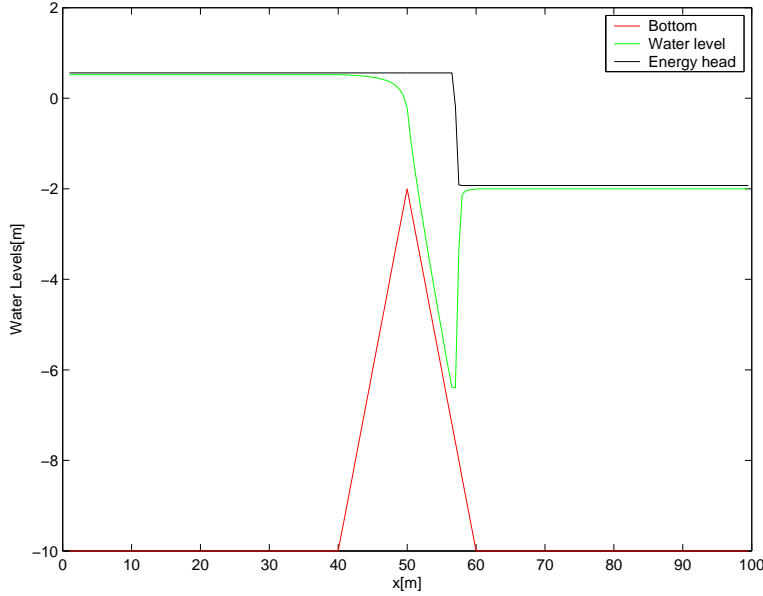


Figure 3.5: 2D model without viscosity, smooth bed

3.6 shows the horizontal velocity distribution, which shows that this scheme meet the requirement mentioned before.

Figure 3.7 shows the velocity vectors.

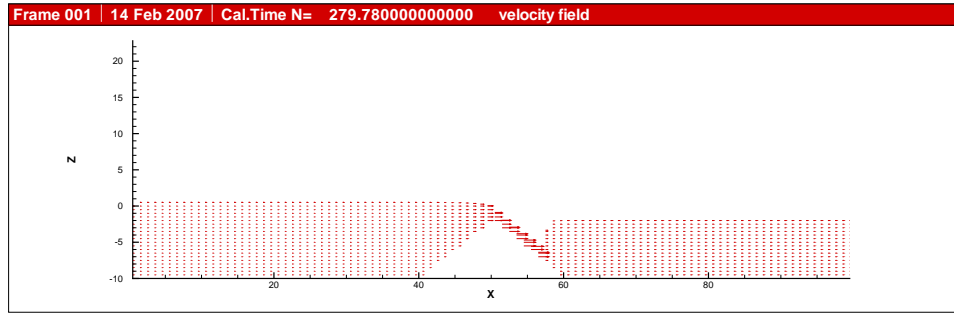


Figure 3.6: 2D model without viscosity, smooth bed, horizontal velocity distribution

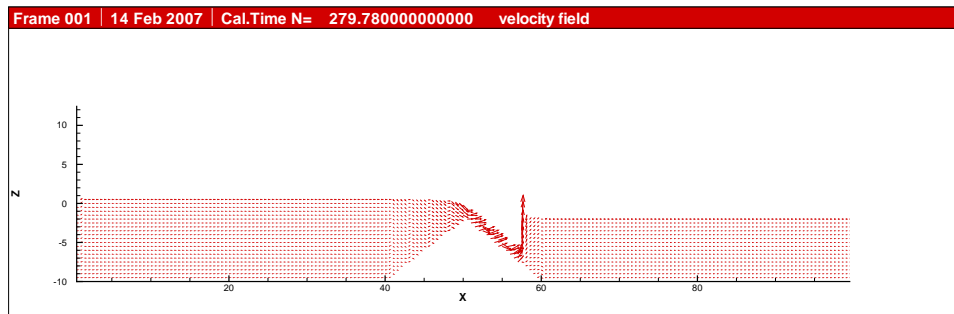


Figure 3.7: 2D model without viscosity, smooth bed, horizontal velocity vector distribution

Chapter 4

Non-hydrostatic 2DV model use pressure gradient as unknown

The model described in this chapter is based on the one developed by Stelling and Van Kester in 2000 [10]. A slightly modified version of that one can be found in M.van Reeuwijk (2002) [14]. The model is based on a new approach for calculating the hydrodynamic pressure and staggered grid. However, the staggered grid used here is different from classic staggered grid. In both approaches, the flow variables (horizontal and vertical velocities u and w) are approximated at the cell interfaces. Unlike the classic staggered grid, which approximates the hydrodynamic pressure q in the cell center, the new approach positions the pressure, and an additional unknown, the vertical pressure gradient, at the cell interface (See Figure 4.1).

4.1 Model definitions

The model is formulated in the same Cartesian co-ordinates just introduced in section 3.2. The new approach positions the pressure at the top of the cell interface and furthermore, introduces the vertical pressure gradient as extra unknown which is known as Hermitian method.

$$\frac{q_k - q_{k-1}}{\Delta z_k} = \frac{1}{2} \frac{\partial q}{\partial z} \Big|_k + \frac{1}{2} \frac{\partial q}{\partial z} \Big|_{k-1} \quad (4.1)$$

4.2 Governing equations

The governing equations still are the Reynolds-averaged Navier-Stokes equations for incompressible fluid the same as described in Section 3.1. But here, the pressure $p(x, z, t)$ can be decomposed into the sum of the hydrostatic

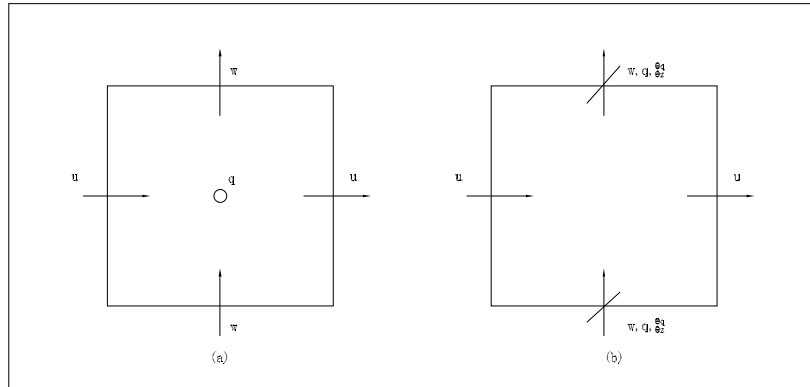


Figure 4.1: Definition sketch of a classic staggered grid (a) and the staggered grid for the new approach (b).

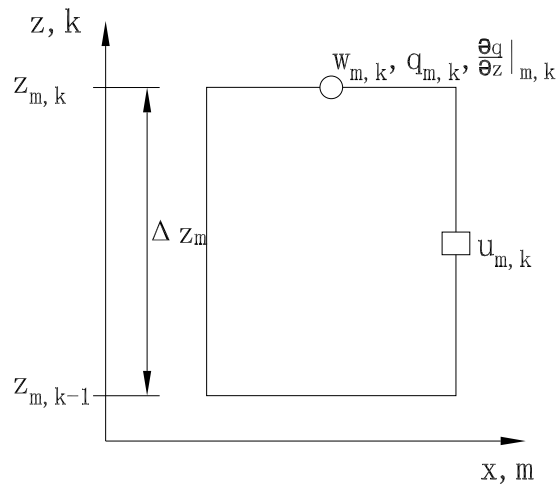


Figure 4.2: Cell definition sketch of the staggered grid

and non-hydrostatic components.

$$p = p_h + q \quad (4.2)$$

The hydrostatic pressure component is determined from the vertical momentum by neglecting the convective acceleration and the viscous terms. The hydrodynamic(or non-hydrostatic) pressure q is the contribution to the total pressure due to acceleration of the fluid. This gives:

$$p(x, z, t) = g[\zeta(x, t) - z] + q(x, z, t) \quad (4.3)$$

By substituting Equ.(4.3) into (3.1) and (3.2) we can obtain:

$$\frac{\partial u}{\partial t} + u \frac{\partial u}{\partial x} + w \frac{\partial u}{\partial z} = -g \frac{\partial \zeta}{\partial x} - \frac{\partial q}{\partial x} + v^h \frac{\partial^2 u}{\partial x^2} + \frac{\partial}{\partial z} \left(v^v \frac{\partial u}{\partial z} \right) \quad (4.4)$$

$$\frac{\partial w}{\partial t} + u \frac{\partial w}{\partial x} + w \frac{\partial w}{\partial z} = -\frac{\partial q}{\partial z} + v^h \frac{\partial^2 w}{\partial x^2} + \frac{\partial}{\partial z} \left(v^v \frac{\partial w}{\partial z} \right) \quad (4.5)$$

4.3 Discretisation of the equations

The discretisation is also based on staggered grid. The horizontal momentum equation is discretised as:

$$\begin{aligned} u_{m,k}^{n+1} = & u_{m,k}^n - \Delta t ADV(u_{m,k}^n, u_{m,k}^{n+1}) + \Delta t HV(u_{m,k}^n) \\ & + \Delta t VV(u_{m,k}^{n+1}) - g \frac{\Delta t}{\Delta x} (\zeta_{m+1}^n - \zeta_m^n) \\ & - \frac{\Delta t}{2} \frac{(q_{m+1,k}^{n+1} + q_{m+1,k-1}^{n+1}) - (q_{m,k}^{n+1} + q_{m,k-1}^{n+1})}{\Delta x} \end{aligned} \quad (4.6)$$

The vertical momentum equation is discretised as:

$$\begin{aligned} w_{m,k}^{n+1} = & w_{m,k}^n - \Delta t ADV(w_{m,k}^n) + \Delta t HV(w_{m,k}^n) \\ & + \Delta t VV(w_{m,k}^n) + \Delta t \frac{\partial q}{\partial z} \Big|_{m,k}^{n+1} \end{aligned} \quad (4.7)$$

The discretisations of the advective and viscous terms are outlined in Appendix B.

The local continuity equation is discretised as:

$$\frac{\Delta z_{mu(m),k}^n u_{m,k}^{n+1} - \Delta z_{mu(m-1),k}^n u_{m-1,k}^{n+1}}{\Delta x} + w_{m,k}^{n+1} - w_{m,k-1}^{n+1} = 0 \quad (4.8)$$

The usage of the mu here implies this is a volume-conserving implementation.

The kinematic boundary condition at the free surface is given by:

$$w_{m,ktop(m)}^{n+1} - \frac{\zeta_m^{n+1} - \zeta_m^n}{\Delta t} - u_{mu(m),ktop(m)}^{n+1} \frac{\zeta_{mu(m)}^n - \zeta_{mu(m)-1}^n}{\Delta x} = 0 \quad (4.9)$$

while at the bottom:

$$w_{m,kbot(m)-1}^{n+1} + u_{mu(m)-1,kbot(m)}^{n+1} \frac{d_{mu(m)}^n - d_{mu(m)-1}^n}{\Delta x} = 0 \quad (4.10)$$

4.4 Solution of the system

The model uses a four-dimensional matrix to store the coefficients of the pressure gradients.

$$\sum_{l=-1}^1 \sum_{o=0}^{kmax} A_{m,k,l,o} \frac{\partial q}{\partial z} \Big|_{m+l,o}^{n+1}$$

In this expression the first two indices represent the location m,k of the equation we concern. The two additional indices l,o are used to relate with any other pressure gradient in the domain. The third index is relative, ranging from -1 to 1. -1 indicates the column to the left, 1 the column to the right, 0 the column where the equation we concern locates. The last index is used to identify the absolute vertical position. A graphical representation of the coefficient matrix is shown in Figure 4.3.

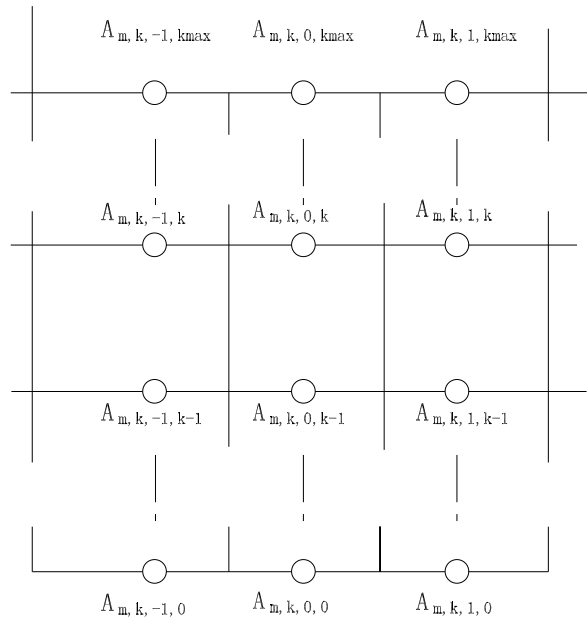


Figure 4.3: The 4D matrix indicates the relation of the equation m,k with its neighbours

Substitution of the momentum equations into the local continuity equation

The pressure gradients are used as primary unknown for the final system. For the horizontal momentum equation, the horizontal pressure gradient can be rewritten as:

$$\begin{aligned}
& \frac{(q_{m+1,k}^{n+1} + q_{m+1,k-1}^{n+1}) - (q_{m,k}^{n+1} + q_{m,k-1}^{n+1})}{2\Delta x} \\
= & \frac{(2q_{m+1,k}^{n+1} - (q_{m+1,k}^{n+1} - q_{m+1,k-1}^{n+1})) - (2q_{m,k}^{n+1} - (q_{m,k}^{n+1} - q_{m,k-1}^{n+1}))}{2\Delta x} \\
= & \frac{(q_{m+1,k}^{n+1} - \frac{\Delta z_{m+1,k}^n}{4} (\frac{\partial q}{\partial z}|_{m+1,k}^{n+1} - \frac{\partial q}{\partial z}|_{m+1,k-1}^{n+1})) - (q_{m,k}^{n+1} - \frac{\Delta z_{m,k}^n}{4} (\frac{\partial q}{\partial z}|_{m,k}^{n+1} - \frac{\partial q}{\partial z}|_{m,k-1}^{n+1}))}{\Delta x}
\end{aligned} \tag{4.11}$$

Note that $q_{k_{top}}^{n+1} = 0$ along the free surface. Therefore, $q_{m,k}^{n+1}$ can be expressed as a sum of vertical pressure gradients by:

$$q_{m,k}^{n+1} = -\frac{1}{2} \sum_{l=k+1}^{ktop(m)} \Delta z_{m,l}^n \left(\frac{\partial q}{\partial z}|_{m,l}^{n+1} + \frac{\partial q}{\partial z}|_{m,l-1}^{n+1} \right) \tag{4.12}$$

Equation 4.12 implies the horizontal momentum equation is coupled to all pressure gradients towards the free water surface(See Figure 4.4). With the help of 4D matrix, the horizontal momentum equation can be expressed as follow:

$$u_{m,k}^{n+1} + \sum_{l=0}^1 \sum_{o=0}^{ktop(m)} a u_{m,k,l,o} \frac{\partial q}{\partial z}|_{m+l,o}^{n+1} = r u_{m,k} \tag{4.13}$$

The vertical momentum equation, which is already expressed in the terms of the vertical pressure gradient, needs no further treatment. It is can be formulated as:

$$w_{m,k}^{n+1} + a w_{m,k} \frac{\partial q}{\partial z}|_{m,k}^{n+1} = r w_{m,k} \tag{4.14}$$

By substituting the horizontal and vertical momentum equations (4.13) and (4.14) into the local continuity equation (4.8), the final system of linear equations are obtained, which is given by:

$$\begin{aligned}
& \frac{\Delta z_{mu(m),k}^n}{\Delta x} \left(r u_{m,k} - \sum_{l=0}^1 \sum_{o=0}^{ktop(m)} a u_{m,k,l,o} \frac{\partial q}{\partial z}|_{m+l,o}^{n+1} \right) \\
& - \frac{\Delta z_{mu(m-1),k}^n}{\Delta x} \left(r u_{m-1,k} - \sum_{l=0}^1 \sum_{o=0}^{ktop(m-1)} a u_{m-1,k,l,o} \frac{\partial q}{\partial z}|_{m+l-1,o}^{n+1} \right) \\
& + \left(r w_{m,k} - a w_{m,k} \frac{\partial q}{\partial z}|_{m,k}^{n+1} \right) - \left(r w_{m,k-1} - a w_{m,k-1} \frac{\partial q}{\partial z}|_{m,k-1}^{n+1} \right) = 0 \tag{4.15}
\end{aligned}$$

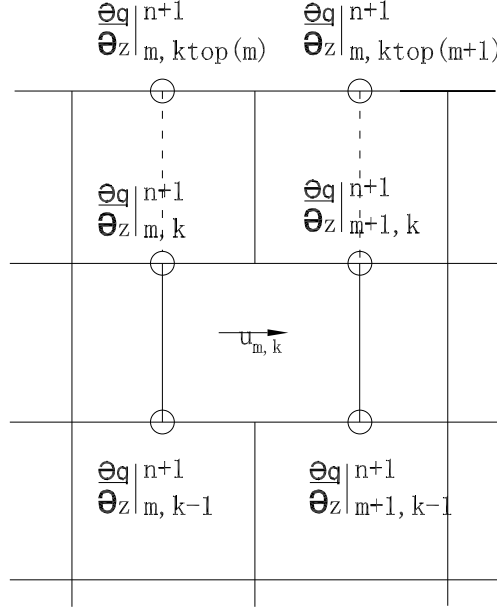


Figure 4.4: The horizontal momentum equation is coupled to all vertical pressure gradients towards the water surface

Equation (4.15) can be written in the form of:

$$\sum_{l=-1}^1 \sum_{kbot(m)}^{ktop(m)} \mathbf{A}_{m,k,l,o} \frac{\partial q}{\partial z} \Big|_{m+l,o}^{n+1} = r_{m,k} \quad (4.16)$$

In the vertical, there are only $ktop - kbot$ continuity equations, so Equation (4.16) represents $ktop - kbot$ linear equations. However, the number of unknowns equals $ktop - kbot + 1$ in the vertical, so another relation is needed to close the system. The kinematic boundary condition at the bottom (4.10) is used for this purpose.

$$rw_{m,kbot(m)-1} - aw_{m,kbot(m)-1} \frac{\partial q}{\partial z} \Big|_{m,kbot(m)-1}^{n+1} + \left(ru_{m^*,kbot(m)} - \sum_{l=0}^1 \sum_{o=1}^{ktop(m^*)} au_{m^*,k,l,o} \frac{\partial q}{\partial z} \Big|_{m^*+l,o}^{n+1} \right) \frac{d_{m^*+1} - d_{m^*}}{\Delta x} = 0 \quad (4.17)$$

where $m^* = mu(m) - 1$

This closed system can be solved by Gauss-elimination.

4.5 Boundary conditions

Up to this point, the calculation has been restricted to interior cells. The Navier-Stokes equations (4.4) and (5.3) are of course incomplete without boundary conditions. In general there are two types of boundary conditions: closed and open (Stelling, 1984) [9]. Closed boundaries are land-water boundaries; they are physical because they relate to a really existing boundary. Open boundaries are mathematical; they are introduced to restrict the size of the domain of the problem.

Closed boundaries:

At closed boundaries the following boundary conditions are given:

$$u_{\perp} = 0, \quad (4.18)$$

$$(1 - \alpha)u_{\parallel} + \Delta\alpha \frac{\partial}{\partial n}u_{\parallel} = 0 \quad (4.19)$$

where u_{\perp} denotes the velocity normal to the boundary, u_{\parallel} denotes the velocity parallel to the boundary and $\frac{\partial}{\partial n}$ denotes the derivative normal to the boundary. If $\alpha = 1$ then (4.19) describes a "perfect slip" boundary condition but if $\alpha = 0$ then (4.19) represents a "no slip" boundary condition. In general $\alpha = 1$.

The boundary treatment, near closed boundaries, for the advection terms is as follows:

uu_x :

To avoid both too large dissipative discretizations near the boundary or unstable discretizations, the following procedure for the situation of figure (4.5) are adopted.

$$uu_x = \begin{cases} 0, & \text{if } u_{m,n} \geq 0 \\ u_{m,n}(u_{m+1,n} - u_{m,n})/\Delta x & \text{if } u_{m,n} < 0 \end{cases} \quad (4.20)$$

For the discretization of uu_x the following procedure are adopted for the situation of the figure (4.6):

$$uu_x = \begin{cases} u_{m,n}(u_{m,n} - u_{m-1,n})/\Delta x, & \text{if } u_{m,n} > 0 \\ 0, & \text{if } u_{m,n} \leq 0 \end{cases} \quad (4.21)$$

Open boundaries:

Open boundaries are artificial water-water boundaries that have been arbitrarily drawn somewhere across a wider flow field to restrict the domain of the problem. Open boundaries are an important concept when the domain is not completely closed.

a) Velocity boundary conditions given by:

$$u_{\perp} = f^u(t) \quad (4.22)$$

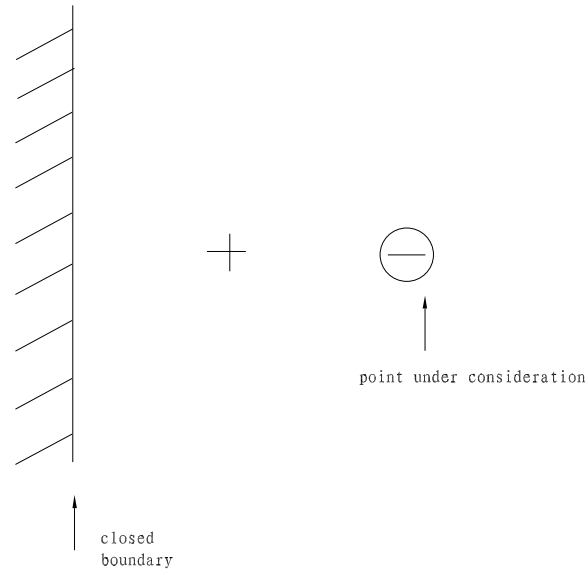


Figure 4.5:

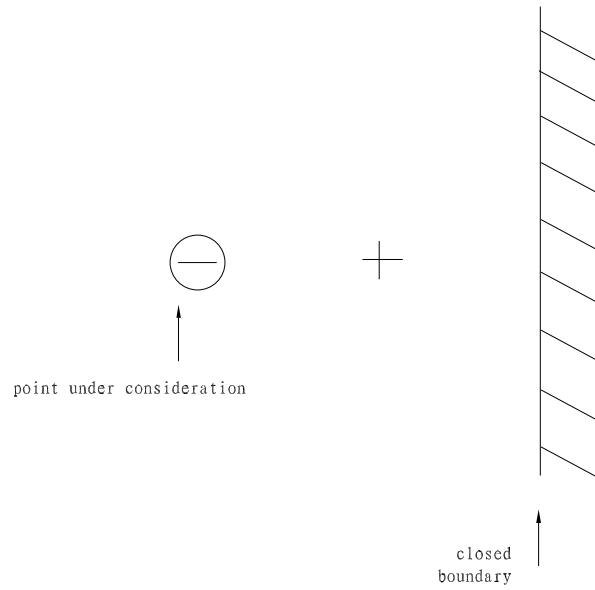


Figure 4.6:

$$u_{\parallel} = 0 \quad (4.23)$$

$$\frac{\partial}{\partial n} u_{\parallel} = 0, \text{ if } \nu \neq 0 \quad (4.24)$$

b) Water level boundary conditions given by:

$$\zeta = f^{\zeta}(t) \quad (4.25)$$

$$u_{\parallel} = 0 \quad (4.26)$$

$$\frac{\partial}{\partial n} u_{\parallel} = 0, \text{ if } \nu \neq 0 \quad (4.27)$$

where (4.23) and (4.26) are prescribed only at inflow, i.e., if u_{\perp} is directed from outside the domain of the problem to inside. Because of the staggered grid, the special boundary procedures are necessary only for the advection terms. The discretization of (4.22)-(4.27) are as following:

a): Velocity boundary conditions (see Figure 4.7):

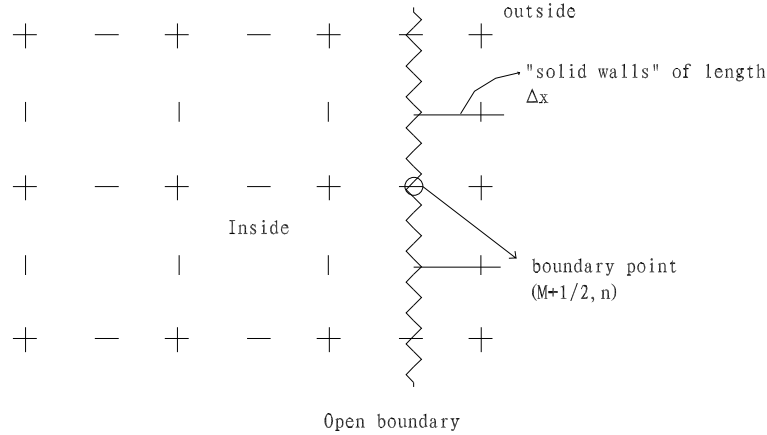


Figure 4.7: Open velocity boundary

$$u^k = f^u(k\tau), \text{ at } M + 1/2, n \quad (4.28)$$

$$w^k = 0, \text{ at } M + 1, n + 1/2 \text{ and } M + 1, n - 1/2 \quad (4.29)$$

$$\zeta_{m+1,n}^k = \zeta_{m,n}^k \quad (4.30)$$

at $m - 1/2, n$, uu_x is approximated by

$$uu_x = \begin{cases} u_{m,n}(u_{m,n} - u_{m-1,n})/\Delta x & \text{if } u > 0 \\ u_{m,n}(u_{m+1,n} - u_{m,n})/\Delta x & \text{if } u \leq 0 \end{cases} \quad (4.31)$$

b): Water level boundary conditions(see Figure 4.8):

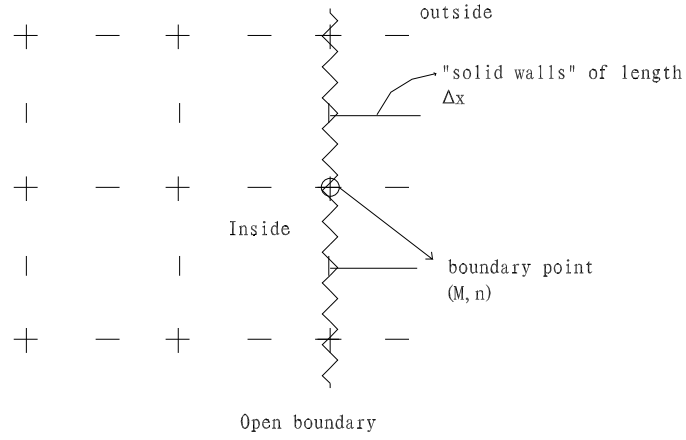


Figure 4.8: Open water level boundary

$$\zeta^k = f^\zeta(k\tau), \text{ at } M, n \quad (4.32)$$

$$w^k = 0, \text{ at } M, n + 1/2 \text{ and } M, n - 1/2 \quad (4.33)$$

at $m - 1/2, n$, uu_x is approximated by

$$uu_x = \begin{cases} u_{m,n}(u_{m,n} - u_{m-1,n})/\Delta x & \text{if } u > 0 \\ 0 & \text{if } u \leq 0 \end{cases} \quad (4.34)$$

at $m - 1\frac{1}{2}, n$, uu_x is approximated by

$$uu_x = \begin{cases} u_{m,n}(u_{m,n} - u_{m-1,n})/\Delta x & \text{if } u > 0 \\ u_{m,n}(u_{m+1,n} - u_{m,n})/\Delta x & \text{if } u \leq 0 \end{cases} \quad (4.35)$$

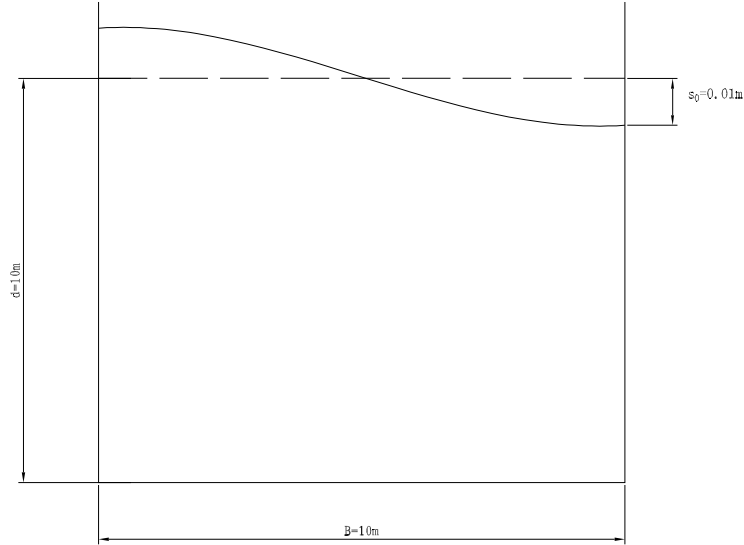


Figure 4.9: Geometry of the basin

4.6 Numerical examples

4.6.1 Standing wave in a closed basin

This example demonstrates the correct prediction of the period of a standing non-breaking non-hydrostatic wave in a closed basin and to show the non-hydrostatic works well. The basin is 10 meters deep and 10 meters wide. So the non-breaking waves have a relatively large ratio of total depth $H = d + \zeta$ to the wave length λ . In such a case the vertical accelerations of the standing wave are of the same order as the horizontal, therefore the hydrostatic pressure assumption does not apply any more. The propagation velocity c is no longer independent of frequency. For sufficiently small wave amplitude, the wave celerity c is coupled by the dispersion relation:

$$c = \frac{\omega_w}{k} = \sqrt{\frac{g}{k} \tanh(kd)} = \sqrt{\frac{g\lambda}{2\pi} \tanh\left(\frac{2\pi d}{\lambda}\right)} \quad (4.36)$$

Here, ω_w represents the angular velocity, k the wave number and d the still water depth.

Note that for shallow water waves ($kd \ll 1$) $\tanh kd$ can be approximated by kd which gives the propagation velocity for shallow water waves:

$$c = \sqrt{gd} \quad (4.37)$$

This means that all the shallow water waves propagate in a same velocity, while for the non-hydrostatic waves, each component has its own velocity. This can be demonstrated later. The 10×10 square basin is discretized with cells $\Delta x = 0.5m, \Delta z = 1.0m$. The initial surface elevation is given by:

$$\zeta(x) = \zeta_0 \cos(2\pi x/\lambda) \tag{4.38}$$

with ζ_0 the amplitude of the standing wave, for this case $\zeta_0=0.01m$. By neglecting the friction, a standing wave of length $\lambda = 2B$ and frequency $f = c/\lambda$ is generated. The calculation is carried out with a time step $\Delta t = 0.01s$. According to the dispersion relation (4.36) the wave period should be 3.59s. Simulation of non-hydrostatic gives results a period that is exactly the same

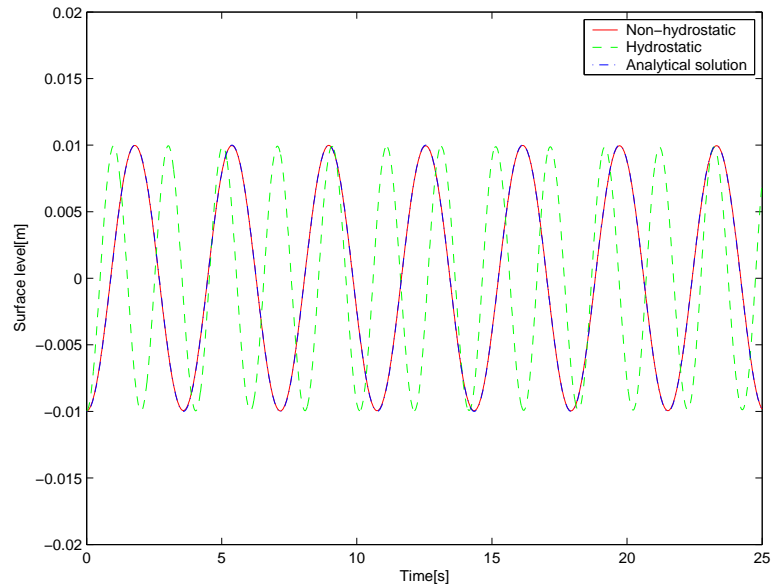


Figure 4.10: Water levels at location $x=10m$ of the standing wave in the closed basin. Comparison with hydrostatic and non-hydrostatic. $\Delta t = 0.01s$

as that given by dispersion relation. While the simulation with hydrostatic produces a totally wrong period (see Figure 4.10).

From Figure 4.11 we can see, while the model with only 1 layer results a period that is slightly large according to the linear dispersion relation, model with 2 layers can predict the period quite well.

If the initial water surface is set as a slope(see Fig 4.12), not a cosine, then the water level at the end of basin will show an irregularity. Based on Fourier Transform analysis, the straight line can be seen as the sum of lots of sine and cosine components. Each one has its own velocity according to the dispersion relation, this produces the irregularity (see Fig 4.13).

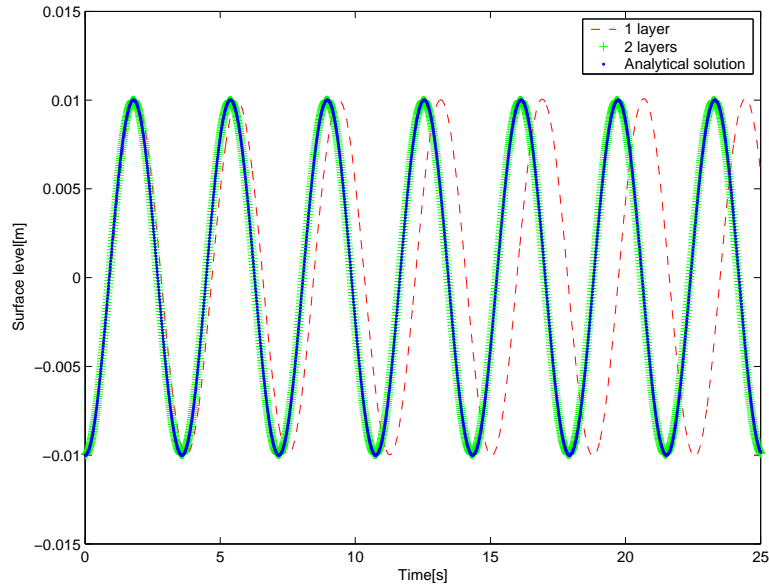


Figure 4.11: Water level at station $x = 10m$ of the standing wave in closed basin. Comparison of the results of 1 layer and 2 layers.

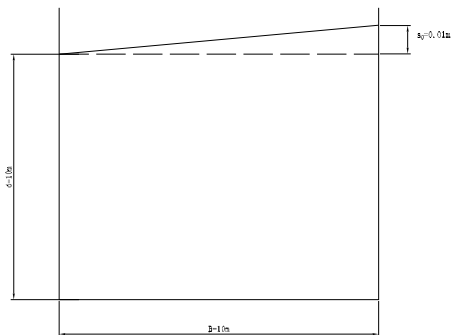


Figure 4.12: Geometry of the basin

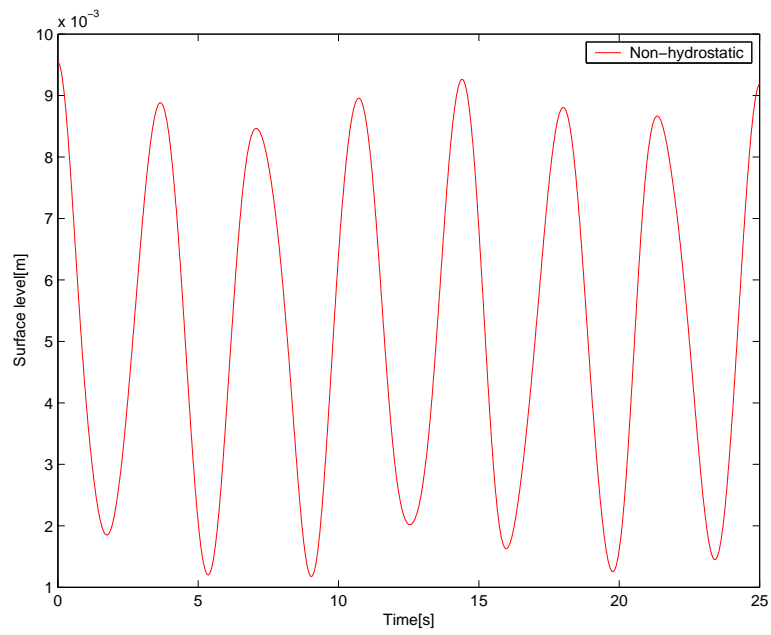


Figure 4.13: Water levels at location $x=10\text{m}$ of the standing wave in the closed basin. $\Delta t = 0.01\text{s}$

Chapter 5

Implicit algorithm for Non-hydrostatic free-surface flow

This one is based on Compact method that taking the effect of non-hydrostatic pressure into account. The technique is described in G.Stelling and M.Zijlema[2003] [11]. This scheme is edge based(see Figure 5.1) in the vertical direction, which makes the zero pressure boundary condition at the free surface approximated very accurately. This approach positions the pressure at the cell interface, and use it as the primary unknown.

5.1 Governing Equations

For the grid in Figure 5.1 , the following equations are to be solved numerically:

1. Continuity equation:

$$\frac{\partial u}{\partial x} + \frac{\partial w}{\partial z} = 0 \quad (5.1)$$

2. Horizontal momentum equation:

$$\frac{\partial u}{\partial t} + u \frac{\partial u}{\partial x} + w \frac{\partial u}{\partial z} = -g \frac{\partial \zeta}{\partial x} - \frac{\partial q}{\partial x} + v^h \frac{\partial^2 u}{\partial x^2} + \frac{\partial}{\partial z} \left(v^v \frac{\partial u}{\partial z} \right) \quad (5.2)$$

3. Vertical momentum equation:

$$\frac{\partial w}{\partial t} + u \frac{\partial w}{\partial x} + w \frac{\partial w}{\partial z} = -\frac{\partial q}{\partial z} + v^h \frac{\partial^2 w}{\partial x^2} + \frac{\partial}{\partial z} \left(v^v \frac{\partial w}{\partial z} \right) \quad (5.3)$$

4. Kinematic boundary conditions:

$$w|_{z=-d} = -u \frac{\partial d}{\partial x} \quad (5.4)$$

$$w|_{z=\zeta} = \frac{\partial \zeta}{\partial t} + u \frac{\partial \zeta}{\partial x} \quad (5.5)$$

or integrated continuity equation:

$$\frac{\partial \zeta}{\partial t} + \frac{\partial}{\partial x} \left[\int_{-d}^{\zeta} u dz \right] = 0 \quad (5.6)$$

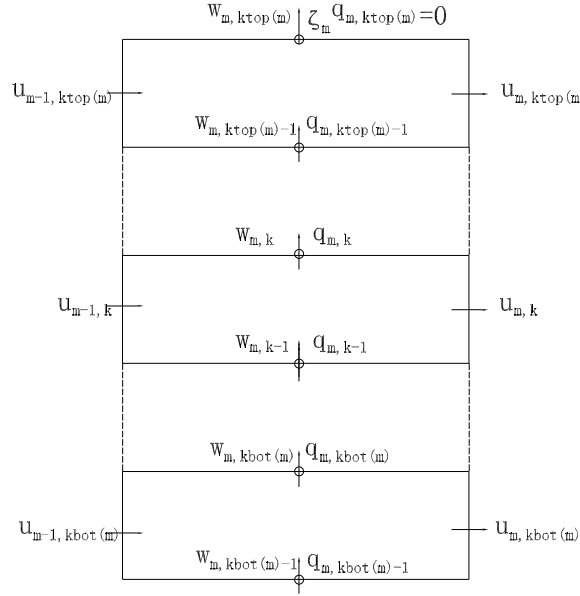


Figure 5.1: The structure of the coefficients and unknowns of the implicit approach.

In this case, we treat the water level ζ implicitly. In total, if there are M layers along the vertical column, $M = ktop - kbottom + 1$, we have $3M + 2$ unknowns(see Figure 5.1) :

- $M q_{m,k}^{n+1}$, $k = kbottom - 1 \sim ktop - 1$, noting that $q_{m,ktop}^{n+1} = 0$
- $M u_{m,k}^{n+1}$, $k = kbottom \sim ktop$
- $M + 1 w_{m,k}^{n+1}$, $k = kbottom - 1 \sim ktop$
- $1 \zeta_m^{n+1}$

This means we need $3M + 2$ equations to solve these unknowns:

- M horizontal momentum equations

- M vertical momentum equations
- M continuity equations
- the kinematic boundary condition at the bottom and the kinematic boundary condition at the water surface or the integrated continuity equation

5.2 Numerical approximation

Now we have enough equations to solve the unknowns. The next step is how to discretize all these equations:

1. Discretization of the horizontal momentum equations:

$$\begin{aligned} & \frac{u_{i+1/2,k}^{n+1} - u_{i+1/2,k}^n}{\Delta t} + ADV(u_{i+1/2,k}^n, u_{i+1/2,k}^{n+1}) - HV(u_{i+1/2,k}^n) \\ & - VV(u_{i+1/2,k}^{n+1}) - (1 - \theta)g \frac{1}{\Delta x} (\zeta_{i+1}^n - \zeta_i^n) - \theta g \frac{1}{\Delta x} (\zeta_{i+1}^{n+1} - \zeta_i^{n+1}) \\ & + \frac{(q_{i+1,k+1/2}^{n+1} - q_{i,k+1/2}^{n+1} + q_{i+1,k-1/2}^{n+1} - q_{i,k-1/2}^{n+1})}{2\Delta x} = 0 \end{aligned} \quad (5.7)$$

The finite-difference operators ADV, HV, VV represent the advection, horizontal and vertical viscosity terms respectively, see Appendix B.

2. Discretization of the vertical momentum equations: Due to some drawbacks of the Keller-box method when treats the vertical momentum equations, see Appendix C, the compact method is used here. The pressure gradient is coupled to the pressure by:

$$\frac{1}{2} \frac{\partial q}{\partial z} \Big|_k + \frac{1}{2} \frac{\partial q}{\partial z} \Big|_{k-1} = \frac{q_k - q_{k-1}}{\Delta z_k} \quad (5.8)$$

Write it in the recursion form.

$$\frac{\partial q}{\partial z} \Big|_k = 2 \frac{q_k^{n+1} - q_{k-1}^{n+1}}{\Delta z_k} - \frac{\partial q}{\partial z} \Big|_{k-1} \quad (5.9)$$

If we make an assumption that the pressure gradient at the bottom is zero, i.e., $\frac{\partial q}{\partial z} \Big|_{k=k_{bot}-1} = 0$, by substituting $\frac{\partial q}{\partial z} \Big|_{k-1}$ into equation (5.9), all the pressure gradients can be expressed by the pressures. The vertical momentum equation is discretized as:

$$\frac{w_{m,k}^{n+1} - w_{m,k}^n}{\Delta t} + ADV(w_{m,k}^n) + VV(w_{m,k}^n) + HV(w_{m,k}^n) + \sum_{l=k_{bot}-1}^k aw(m, k, 0, l) q_{m,l}^{n+1} = 0 \quad (5.10)$$

3. Discretization of the continuity equations(see Section 5.4):

$$\frac{u_{m,k}^{n+1} dzu(m, k) - u_{m-1,k}^{n+1} dzu(m-1, k)}{\Delta x} + w_{m,k}^{n+1} - w_{m,k-1}^{n+1} = 0 \quad (5.11)$$

4. Discretization of the kinematic boundary conditions:

A discretization for the kinematic condition at the free surface is given by:

$$w_{m,ktop}^{n+1} = \frac{\zeta_m^{n+1} - \zeta_m^n}{\Delta t} + \max(0, u_{m-1,ktop}^{n+1}) \frac{\zeta_m^n - \zeta_{m-1}^n}{\Delta x} + \min(0, u_{m,ktop}^{n+1}) \frac{\zeta_{m+1}^n - \zeta_m^n}{\Delta x} \quad (5.12)$$

whereas at the bottom,

$$w_{m,kbottom-1}^{n+1} = -\max(0, u_{m-1,kbottom}^{n+1}) \frac{d_m - d_{m-1}}{\Delta x} - \min(0, u_{m,kbottom}^{n+1}) \frac{d_{m+1} - d_m}{\Delta x} \quad (5.13)$$

5. discretization of the integrated continuity equation:

The discretization for the integrated continuity equation takes the following form:

$$\zeta_m^{n+1} = \zeta_m^n - \frac{\Delta t}{\Delta x} \left[\sum_{k=kbot(m)}^{ktop(m)} dzu(m, k) u_{m,k}^{n+1} - \sum_{k=kbot(m-1)}^{ktop(m-1)} dzu(m-1, k) u_{m-1,k}^{n+1} \right] \quad (5.14)$$

5.3 Sequence of the computation

1. From $kbottom$ to $ktop$, with the help of 4D matrix, each u^{n+1} in Equation (5.7) can be written in the form of:

$$u_{m,k}^{n+1} + \sum_{l=-1}^1 Au_{m,k,l,o} \zeta_{m+l}^{n+1} + \sum_{l=-1}^1 \sum_{o=kbottom-1}^{ktop} Au_{m,k,l,o} q_{m+l,o}^{n+1} = ru_{m,k} \quad (5.15)$$

2. Substitute $u_{m-1,kbottom}^{n+1}$ and $u_{m,kbottom}^{n+1}$ into Equation (5.13), and reconstruct it and eqn. 5.10, the expression of $w_{m,k}^{n+1}$ can be given by:

$$w_{m,k}^{n+1} + \sum_{l=-1}^1 \sum_{o=kbottom-1}^{ktop} Aw_{m,k,l,o} q_{m+l,o}^{n+1} = rw_{m,k} \quad (5.16)$$

where k varies from $kbottom - 1$ to $ktop$

3. Thereafter, Equations (5.15),(5.16) are substituted into Equation (5.11). A linear system of equations for q^{n+1} is obtained, whose form likes:

$$\sum_{l=-1}^1 \sum_{kbot(m)-1}^{ktop(m)-1} \mathbf{A}_{m,k,l,o} q_{m+l,o}^{n+1} = r_{m,k} \quad (5.17)$$

4. By substituting $u_{m-1,k}^{n+1}$ and $u_{m,k}^{n+1}$ into eqn. (5.12) or (5.14), we can get another relation equation about the pressure and the water surface level ζ . The final system is closed now and can be solved by Gaussian elimination.
5. The obtained system can be solved by Gauss-elimination.
6. Compute u^{n+1} by substitution of q^{n+1} and ζ^{n+1} into Equation (5.15).
7. Compute w^{n+1} by substitution of q^{n+1} into Equation (5.16).
8. If $\theta = 0$, compute ζ^{n+1} by substitution of w^{n+1} into Equation (5.12) or alternatively from Equation (5.11).

The structure of the system is schematized in Figure (5.2).

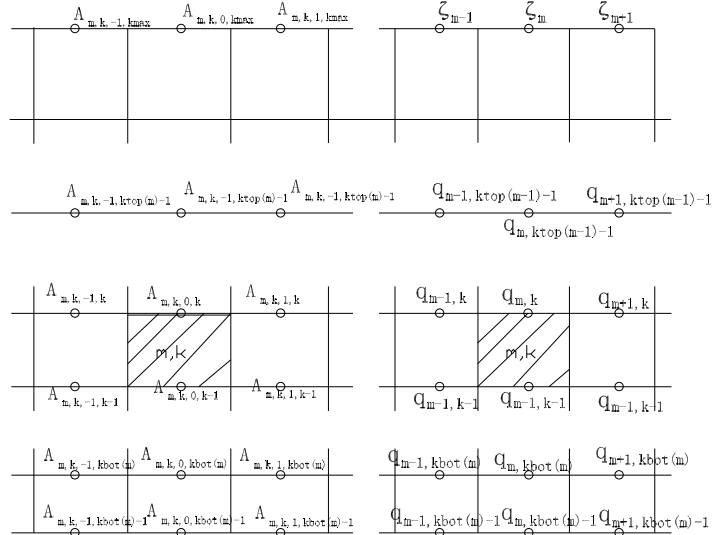


Figure 5.2: The structure of the coefficients and unknowns of the implicit approach.

5.4 Consideration of the bottom

In a full cells z-coordinate model, the water column is sliced into different layers with horizontal planes. Although the vertical spacing Δz may vary in the vertical direction, each layer has the same thickness. Depending on the water depth, the number of grid points in the vertical direction varies. Shallow areas have fewer vertical grid points than deep areas do. When using partial cells method in z-level models, a better approximation of the bottom topography can be got. Instead of the thickness of the layer, the difference between the top of the layer and the real physical bottom is used as the bottom cell thickness, which is generally smaller than the layer thickness. Now the thickness at the two sides of the cell are not the same any longer near the bottom, where the local continuity equation should be treated carefully. Meanwhile, for solid walls, the impermeability condition should be specified, i.e. velocity normal to the wall is zero. Two indexes are introduced, $kbotu(m)$ and $dzu(m, k)$. The $kbotu(m)$ is used to identify the lowest position of the non-zero horizontal velocity, which is given by:

$$kbotu(m) = \max(kbot(m), kbot(m + 1)) \quad (5.18)$$

where $kbot(m)$ and $kbot(m + 1)$ indicate the position of the bottom. All the velocities below $kbotu(m)$ are set to zero, which is to fulfill the impermeability condition for solid walls. $dzu(m, k)$ is used to indicate the thickness of the velocity, which equals the thickness of the layer minus the thickness of the solid wall. With the help of these indexes, the local continuity equation at each cell is approximated as follows (see Figure 5.3):

$$\frac{u_{m,k}^{n+1}dzu(m, k) - u_{m-1,k}^{n+1}dzu(m - 1, k)}{\Delta x} + w_{m,k}^{n+1} - w_{m,k-1}^{n+1} = 0 \quad (5.19)$$

5.5 Numerical examples

5.5.1 Oscillating basin

The newly developed model has been validated by testing a standing wave in a closed basin of square domain ($10 \times 10m$) with the inviscid flow approximation. By choosing a relatively small wave length λ compared to the depth h , the hydrostatic approximation is no longer valid. Initially, all velocities are set to zero and the water surface elevation

$$\zeta_0 = 0.01\cos\left(\frac{2\pi}{\lambda}x\right) \quad \text{with} \quad 0 \leq x \leq 10 \quad (5.20)$$

where $\lambda = 20m$ is the wave length. A zero flow condition is used for all the horizontal velocities at the wall boundaries. The computational domain

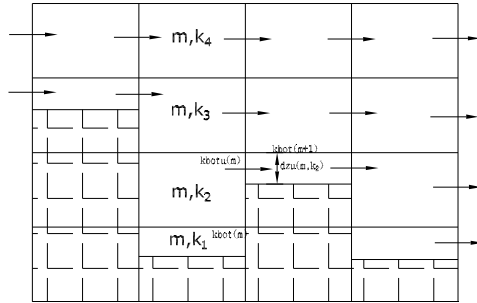


Figure 5.3: Bottom cell schema.

uses a constant grid spacing of $0.5m$ in the longitudinal directions with 20 layers in the vertical direction in order to accommodate the moving free surface. Thus, although a rectangular grid is used in the horizontal direction, the vertical grid is adjusted as a result of free surface movements. The time step $\Delta t = 0.01s$ is used. Here we set $\theta = 0.0$ first, which means the surface level is coupled explicitly. The prediction agrees quite well with the analytical solution (see Figure 5.4).

Figure 5.5 shows the velocity fields at time $t = T/4$, calculated with the non-hydrostatic pressure approximation. If we set $\theta = 1.0$, then the water surface level is fully implicitly coupled in the system. The resulting system is unconditional stable. This can be demonstrated still by the example of oscillating basin, in which $\theta = 1.0$, $\Delta t = 0.1s$ and $\Delta t = 1.0s$. The responding Courant numbers are 2 and 20 respectively, see Figure (5.6).

5.5.2 Hydraulic jump downstream of weir

Weir is the construction widely used in hydraulic engineering. It is very important to investigate the behaviors of the flows over a weir. The ability of the numerical method to simulate discontinuous flows is illustrated. This case has particular characteristics that complicate its numerical modeling (Stelling and Busnelli 2001) [13].

- Discontinuities in the bottom profile.

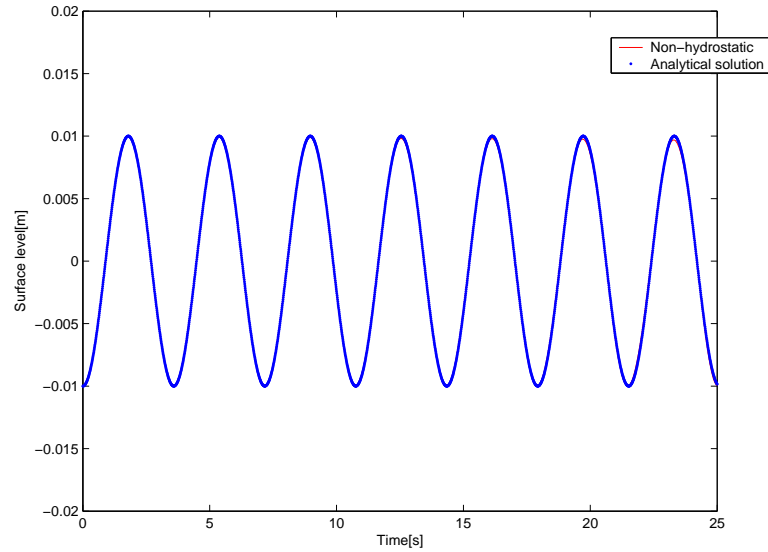


Figure 5.4: Water levels at locations $x=10\text{m}$ of the standing wave in the closed basin. $\theta=0.0$, compact method .

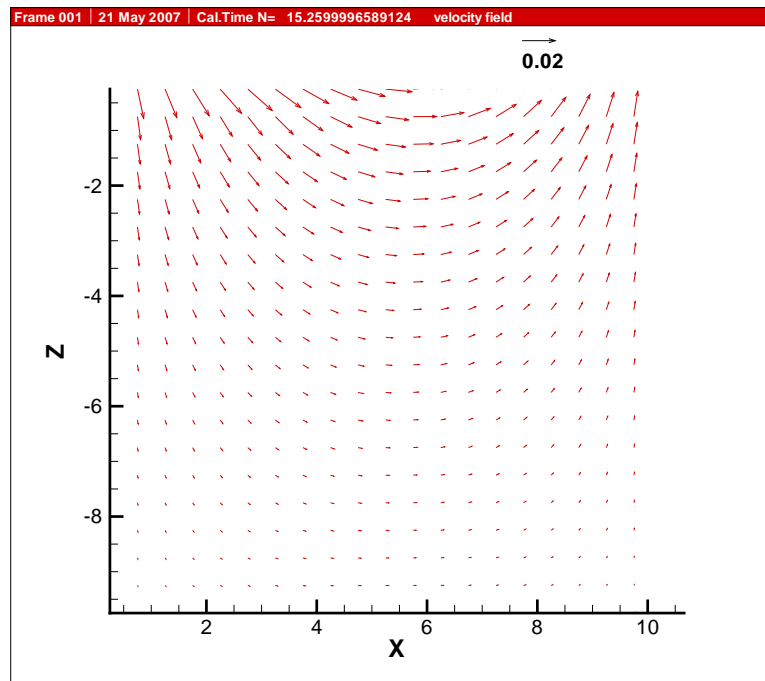


Figure 5.5: Velocity vectors, at time $t = T/4$, with the non-hydrostatic pressure approximation.

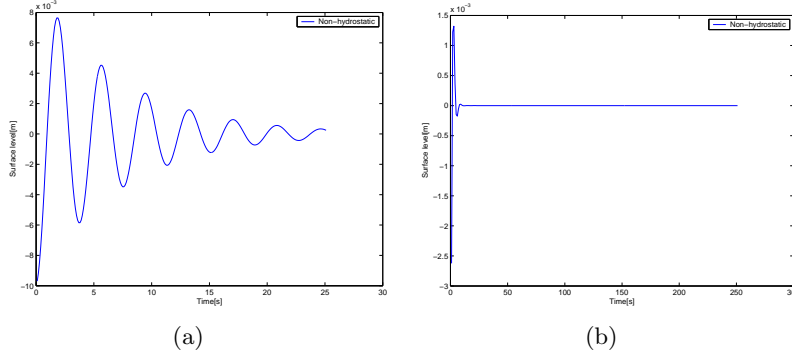


Figure 5.6: Simulation of the oscillating basin with large Courant number, (a) Courant number=2.0 (b) Courant number=20.

- The hydrostatic assumption fails to reproduce the flow mainly because of the departure of the pressures from the hydrostatic values in the region downstream the step.
- The flow changes from sub-critical to super critical (through the critical depth somewhere over the step) and then from supercritical to sub-critical (hydraulic jump).
- Two particular reversal flows should be represented, downstream of the structure (near the bed) and at the hydraulic jump surface (surface roller).

The channel length $L = 3.5m$. The computational domain is discretized with cells of equal size $\Delta x = \Delta z = 0.01m$. At inflow a depth-integrated velocity is prescribed of $0.083m^2/s$ and at outflow a water depth of $0.155m$. A zero flow condition and horizontal water level are used as the initial conditions. The computation was made with timestep $\Delta t = 0.0025s$ and $\theta = 1.0$.

Figure 5.7 shows the water levels and Figure 5.8 and 5.9 illustrates the velocity vectors. From Figure 5.9 we can clearly see that a recirculation zone develops behind the weir and a roller at the hydraulic jump surface is visible. For the experimental data, it refers to [13].

5.5.3 Development of undulation downstream of a weir

A hydraulic jump occurs at the transition from supercritical flow to subcritical flow. The Froude number determines whether the flow is subcritical or supercritical, which is given by:

$$F = \frac{U}{\sqrt{gh}} \quad (5.21)$$

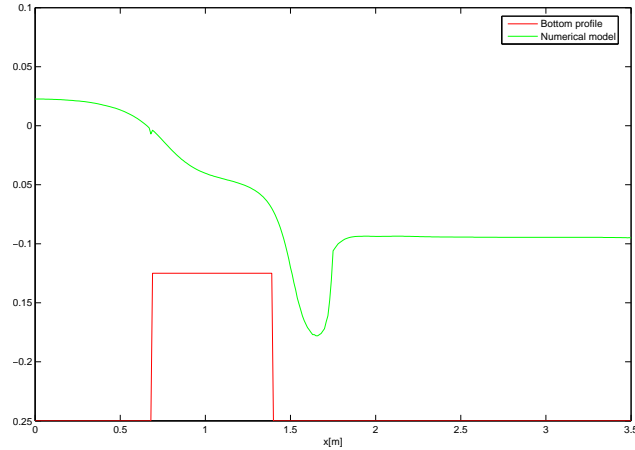


Figure 5.7: Water level

where U = mean flow velocity, h = water depth. Supercritical flow occurs for $Fr > 1$ and is characterized by high velocities and low water depths. Subcritical flow occurs for $Fr < 1$ and is characterized by low velocities and high water depths. An undular hydraulic jump occurs at Froude numbers a little larger than 1 and is characterized by free surface waves. A special case of the undular hydraulic jump is the formation of undulations behind a weir. Three flow regimes are distinguished by Kolkman(1989) [6] for the flow over a weir(see Figure 5.10):

- Free flow(perfect weir). The flow above the weir becomes supercritical and is independent of the downstream water depth. Downstream of the weir a hydraulic jump can occur at some distance.
- Transition zone. This is the transition from free flow to submerged flow, where surface waves develop downstream of the weir.
- Fully submerged flow. The water surface is almost horizontal, the flow above the weir is subcritical and depends on the upstream and downstream water depth.

Starting from the free flow, the transition zone is reached by increasing the downstream water depth. Fully submerged flow is reached by further increasing the downstream water depth. It is difficult to determine the correct Froude number between the end of the weir and the first wave trough, because a recirculation zone develops behind the weir and then the flow is not uniform over the depth. So the Froude number at the end of the weir is used as a parameter to determine whether the undulation

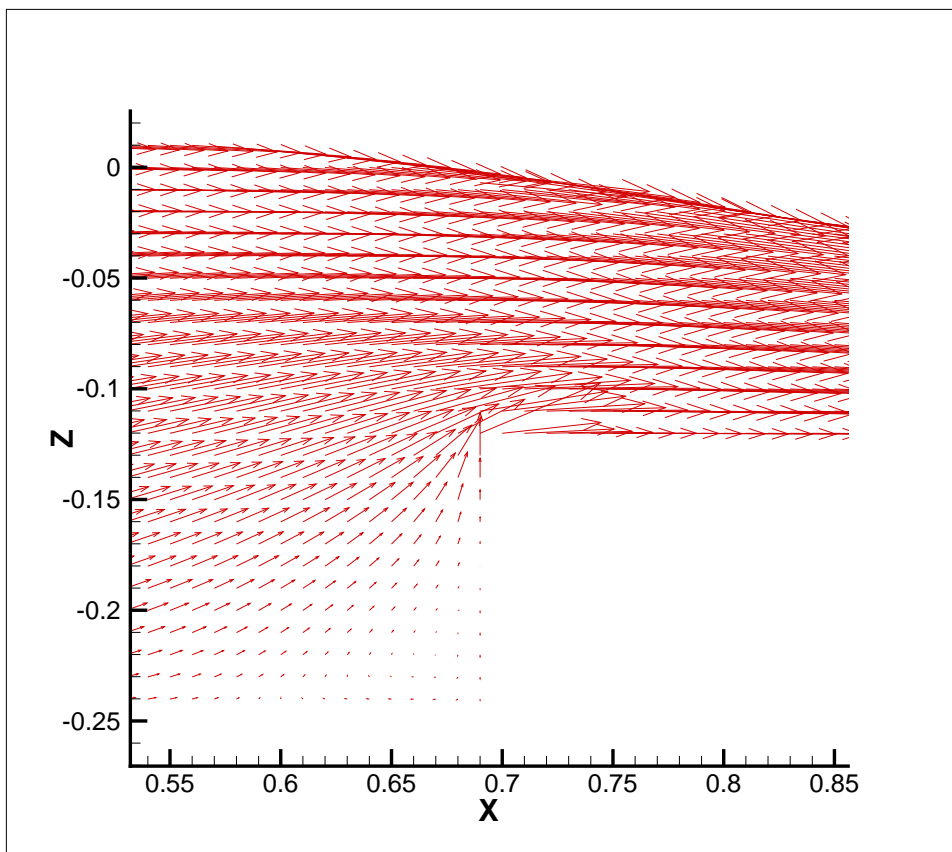


Figure 5.8: Velocity vectors in front of the weir

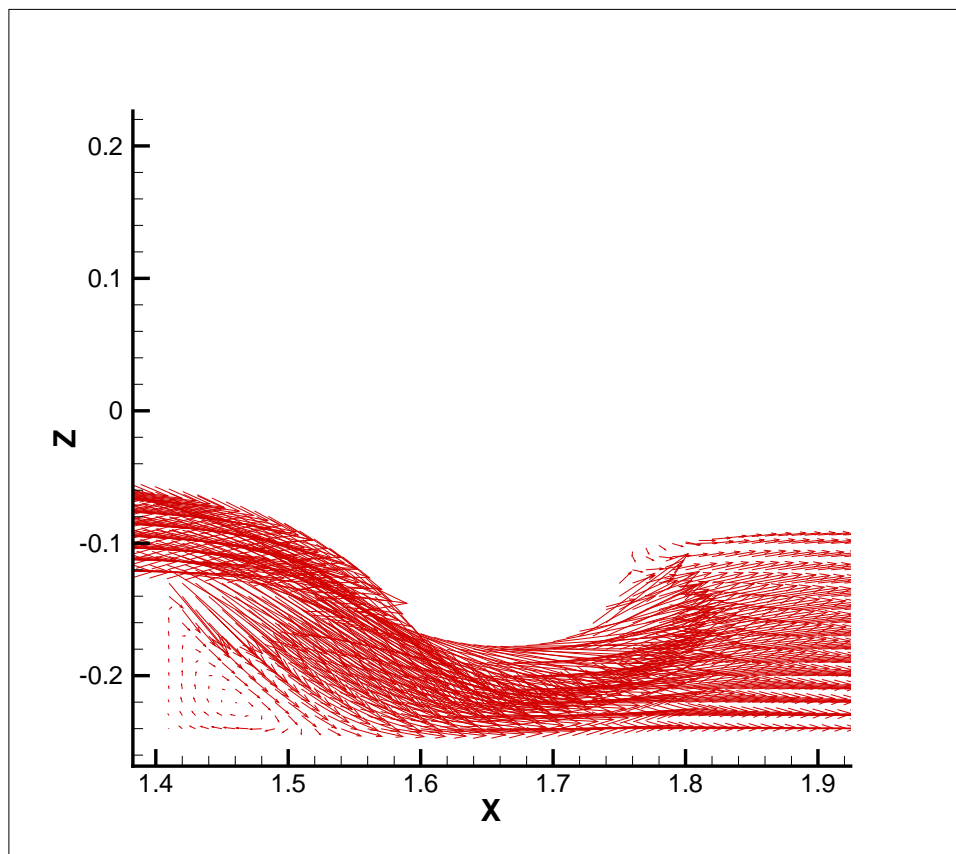


Figure 5.9: Velocity vectors behind the weir

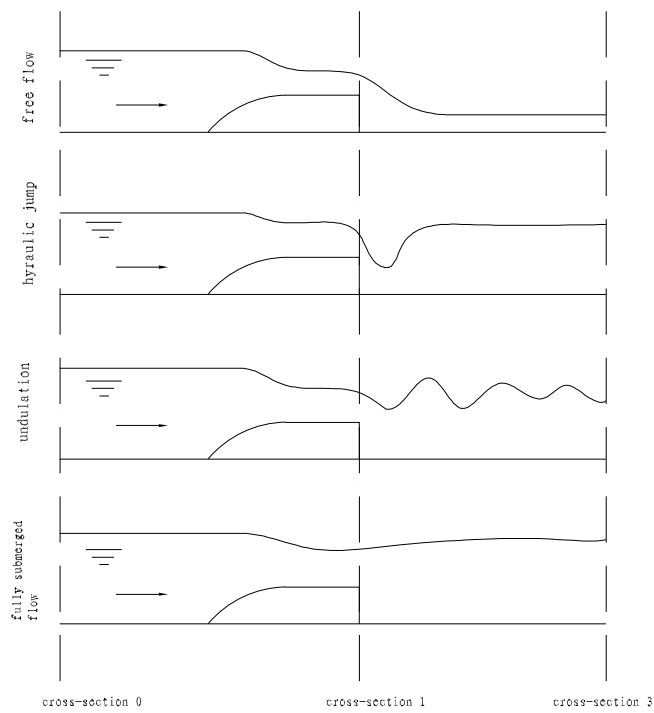
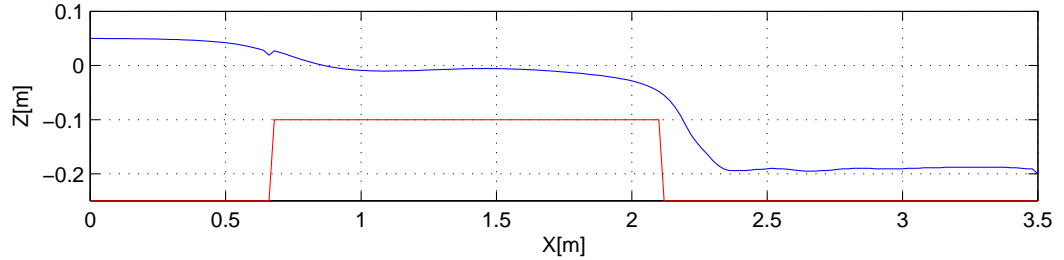
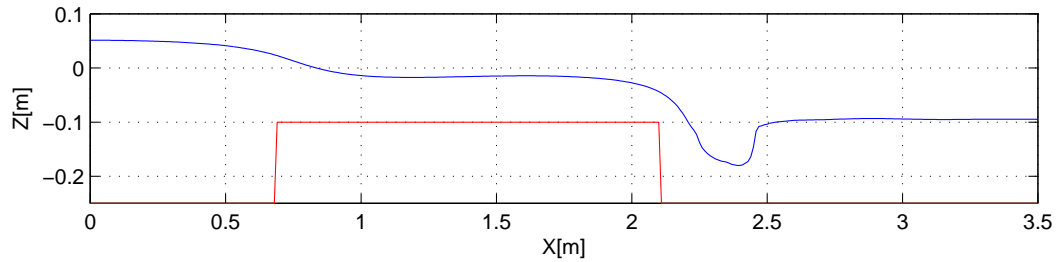


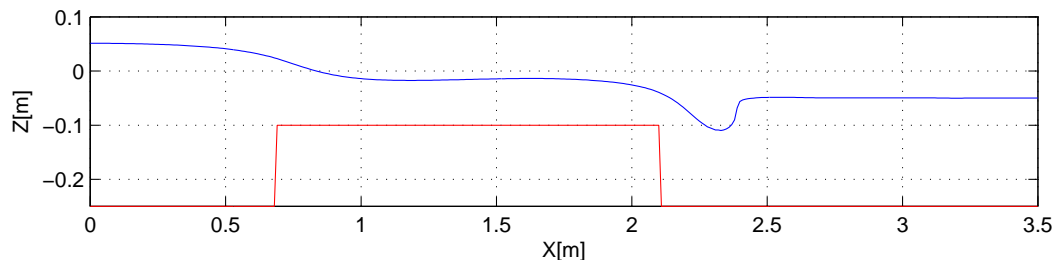
Figure 5.10: Flow regimes over a weir, type of flow regime depends on the degree of submergence.

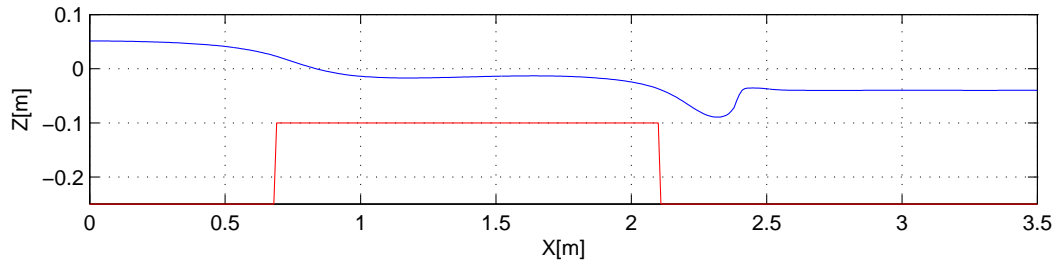
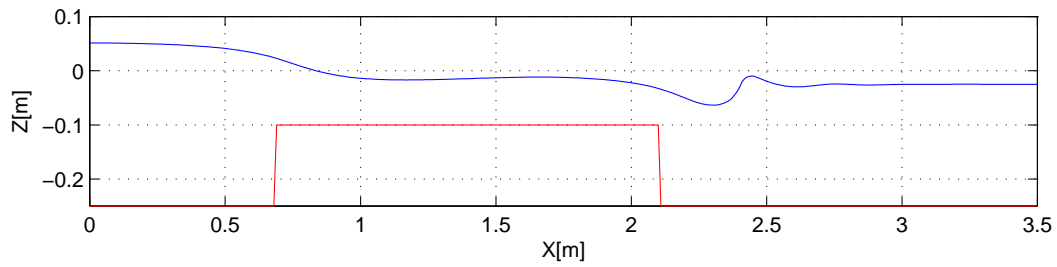
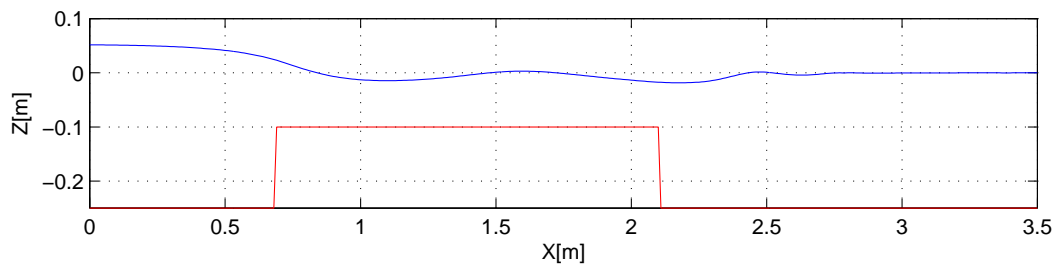
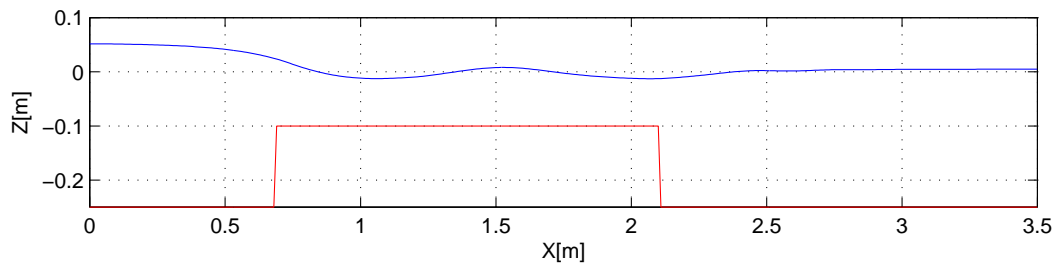
(a) Downstream water level = -0.20m, $Fr=2.23$, Free flow(b) Downstream water level = -0.095m, $Fr=2.98$, Hydraulic jump

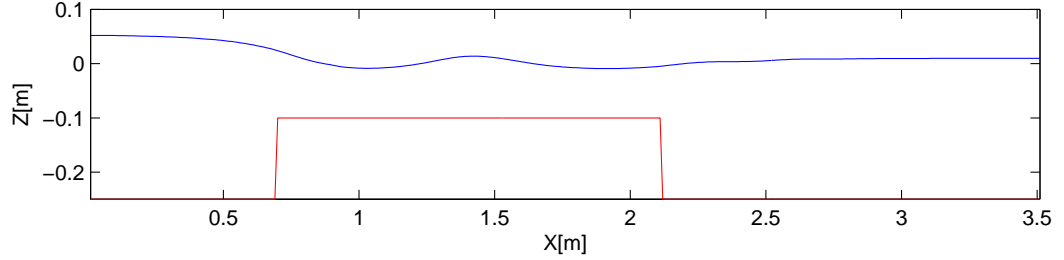
occurs or not. For a certain range of the Froude number ($F=1-1.7$) undulations occur, for higher Froude number the undular jump transforms into a classical jump.

Occurrence of undulations

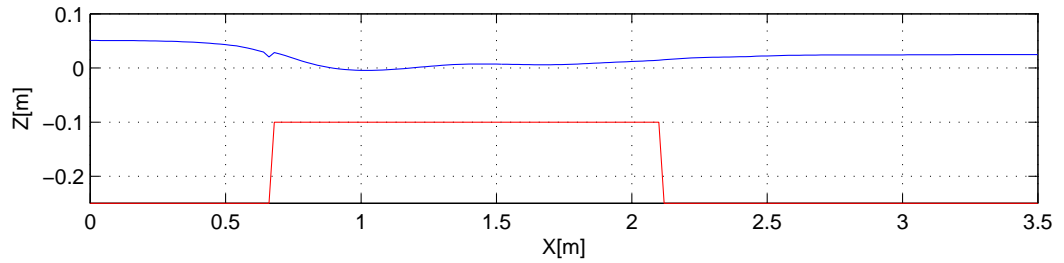
The input parameters for this model are the downstream water depth and the discharge. Numerical simulations (taking viscosity into account) are conducted for the same discharge but for different downstream water depth. In this way, the different approaches can be evaluated by comparing the results for the occurrence of undulations.

(c) Downstream water level = -0.05m, $Fr=1.78$, Hydraulic jump

(d) Downstream water level = -0.04m, $Fr=1.68$, Hydraulic jump(e) Downstream water level = -0.025m, $Fr=1.52$, Undulation(f) Downstream water level = 0.0m, $Fr=1.12$, Undulation(g) Downstream water level = 0.005m, $Fr=1.03$, No Undulation behind the weir



(h) Downstream water level =0.01m, Fr=0.903, No Undulation behind the weir



(i) Downstream water level =0.025m, Fr=0.684, Fully submerged

Figure 5.11: The water profiles of all the conducted numerical experiments

	downstream water level (m)	Description
a	-0.20	Free flow
b	-0.095	Classical hydraulic jump
c	-0.05	Classical hydraulic jump
d	-0.04	Classical hydraulic jump
e	-0.025	Undulation behind the weir
f	0.0	Undulation behind and above the weir
g	0.005	Undulation above the weir and submerged behind the weir
h	0.010	Undulation above the weir and submerged behind the weir
i	0.025	Fully submerged

Water depth at the end of the weir(m)	Average velocity (m/s)	Froude number	Degree of submergence
0.052	1.60	2.23	0.167
0.0564	1.47	1.98	0.517
0.0606	1.37	1.78	0.667
0.0629	1.32	1.68	0.70
0.0672	1.24	1.52	0.75
0.0825	1.01	1.12	0.833
0.0873	0.95	1.03	0.85
0.0951	0.873	0.903	0.867
0.115	0.725	0.684	0.917

From Figure 5.17 and the table we can see that this model is capable of describing the transition zones from undulations to no undulations. For the abrupt change in bottom profile, undulations occur for Froude number above the end of the weir between 1-1.7. This is in good agreement with the occurrence of the undular jump in literature (Chow 1973) [3]. Undulations occur for degrees of submergence between 0.75 and 0.867, which is also in good agreement with the measurements (between 0.75 and 0.90).

Wave characteristics

For a proper evaluation of the model, the wave characteristics are investigated. To compare with the experimental data, we also employ a weir with a smooth upstream part (sine squared) and a sharp-crested downstream part (see Figure 5.12). In Figure 5.13 a definition sketch is

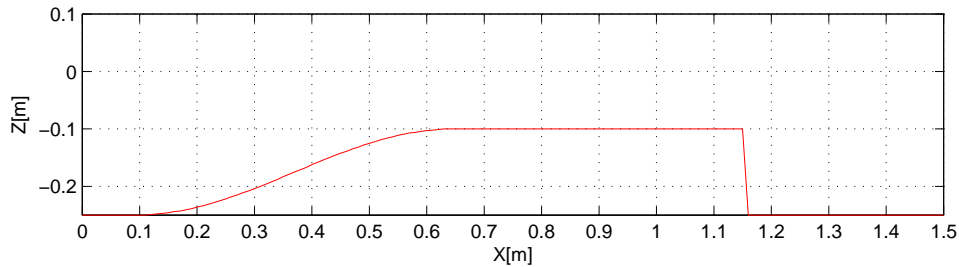


Figure 5.12: Bottom profile.

given for the undulation behind a abruptly changed weir in a channel with a horizontal bottom. The wave length L_1 is given by the distance between the first and second wave trough. The wave height H_1 is given by the distance between the first wave trough and first wave top. This is the biggest wave height due to the sharp drop in water level at the first wave trough. From Figure 5.15, the computational results are plotted against the experimental data, for three different cases (For more details about the experiment, it refers to (Wols,2005)) [1]. The flume is discretized with cells of size $\Delta x = 1.5\text{cm}$, $\Delta z = 2\text{cm}$. The input parameters for this model are, the downstream water depth and the integrated discharge upstream. The flume width is 40cm. The calculation is carried out with a time step $\Delta t = 0.0025\text{s}$ and $\theta = 1.0$. After 5000 time steps the steady state is obtained. From Figure 5.15 we can see, the model predicts the wave length L_1 and wave height H_1 in a good manner. The good agreement with the experiments can only be seen in the first wave zone. However, even for the experiment, the undulations are not stable for some cases. For the same settling, the downstream part of the undulation changed from case to case. Moreover, the undulations also moves a little up and downstream during

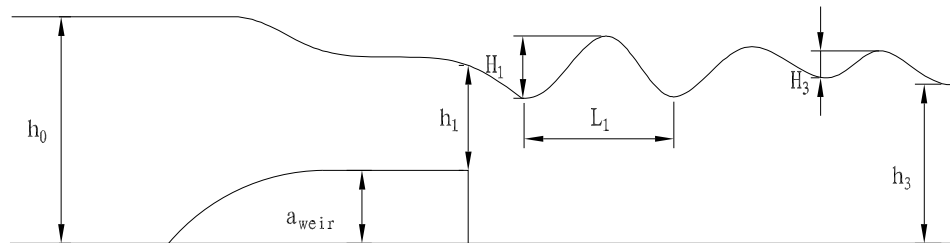
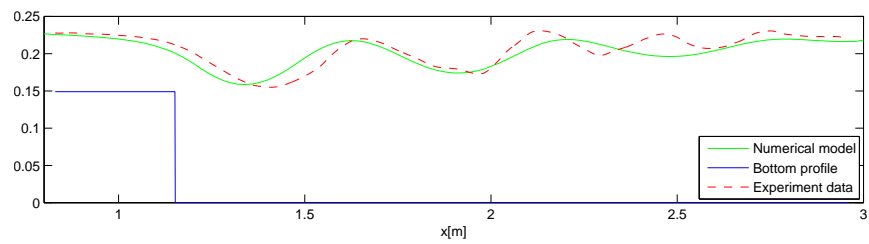
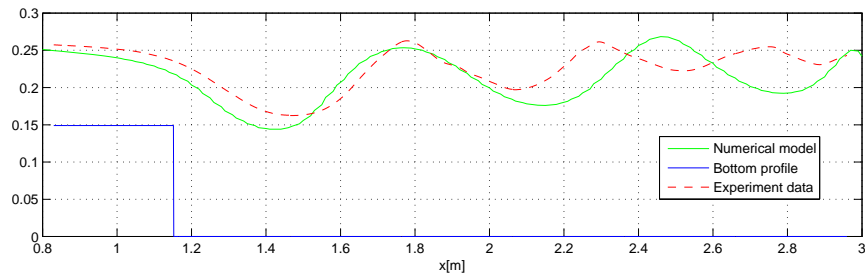


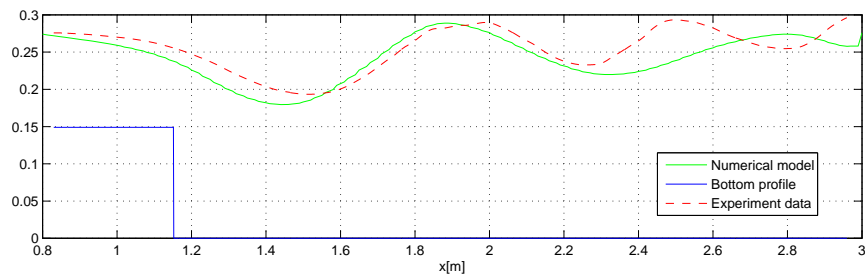
Figure 5.13: Definition of the variables concerning the undulations behind a weir.



(a) Downstream water depth = 0.2183m, $Q=30$ [l/s]



(b) Downstream water depth =0.2418m, $Q=45$ [l/s]



(c) Downstream water depth =0.2758m, $Q=60$ [l/s]

Figure 5.15: The comparison of the water profiles of numerical model with experiments data

the experiment, depending on the natural frequency of the flume. So we have no reason to expect to have the same results as the experiment. Figure 5.16 illustrates the velocity vectors behind the weir. The existence of the recirculation zone is clearly visible. A small recirculation zone develops directly behind the weir. Under each wave crest a bigger recirculation zone can be seen. The direction of the velocities at the water surface agree with the slope of the water level. The highest velocities are observed near the free surface.

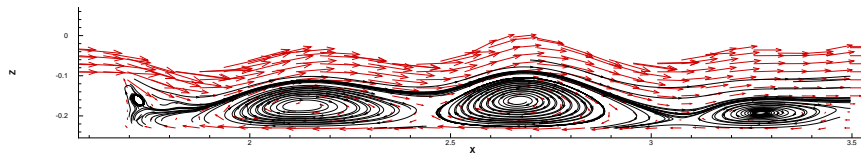
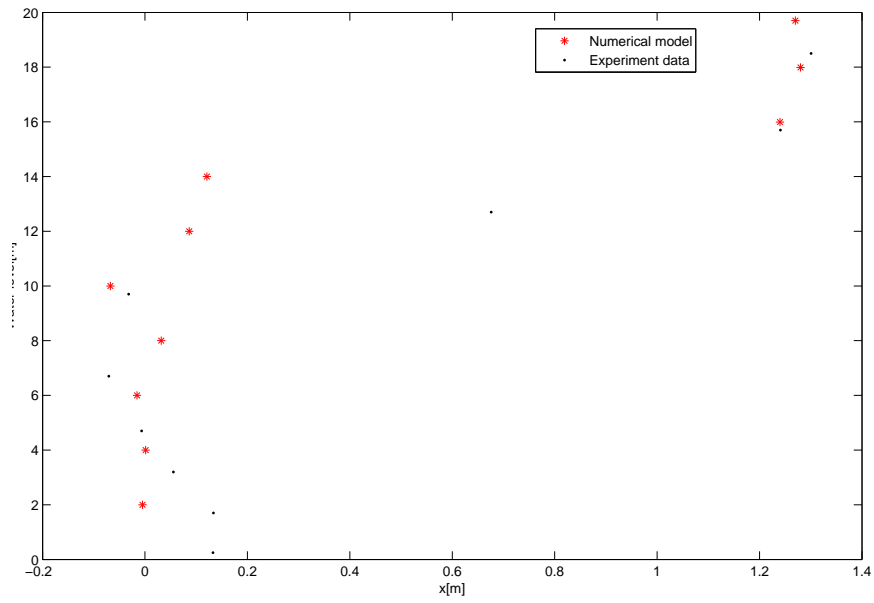


Figure 5.16: Velocity vectors behind the weir, $Q=30$ [l/s].

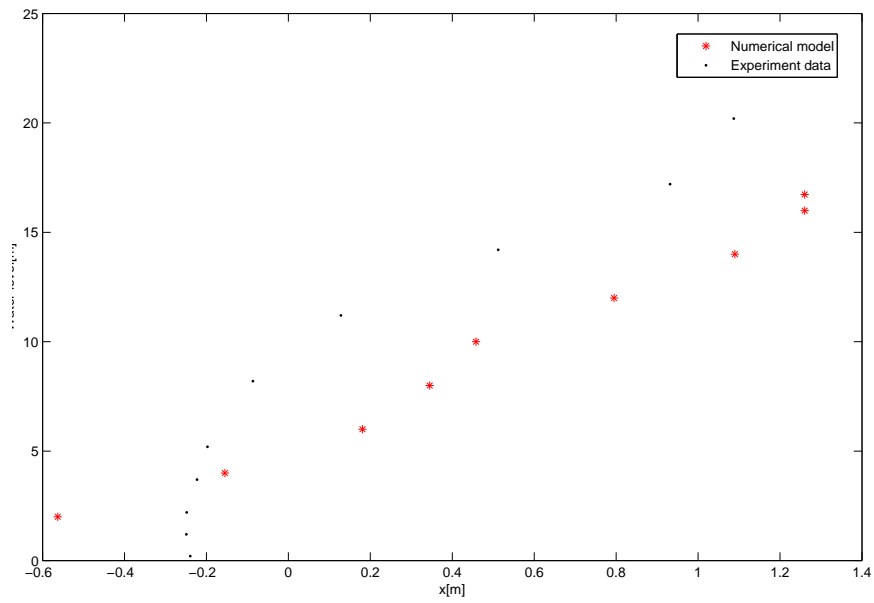
Velocity profiles The velocity profiles are measured by the LDA-device in experiment. From Figure (5.17) we can see, the vertical structure of the horizontal velocity agrees quite well with the experimental data just behind the weir. At the first wave trough, the predicted velocity gradient is larger and the velocity reverse point is lower than that in the experiment. For the profile at location of first wave top, the numerical results shows quite good agreement with the experimental data for the upper part. While for the lower part, the numerical velocity is larger.

5.5.4 The failure of the $k - \varepsilon$ model

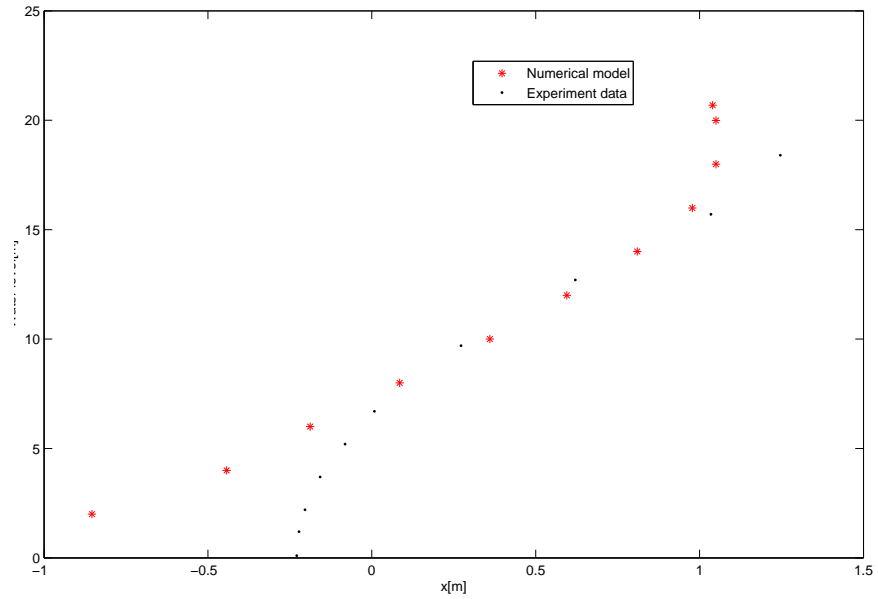
In the previous section, the last three numerical experiment (Figure 5.15) are conducted without taking viscosity into account. If the viscosity is added to the model by $k - \varepsilon$ model, the computational results become much different from the experimental data. Neither the wave length L_1 nor the wave height H_1 can be well predicted. The first wave becomes much smaller and much shorter than that of the experiment and the following waves damp out quite fast in the downstream zone (see Figure 5.18). The recirculation zone under the wave top disappears (see Figure 5.19). For the prediction of wave characteristics of undulation, the $k - \varepsilon$ model fails. The viscosity terms have the function to damp the wave out. So the standard $k - \varepsilon$ turbulence closure model will introduce errors in the region where non-hydrostatic pressure is dominant.



(a) At $x=1.17\text{m}$



(b) At $x=1.41\text{m}$



(c) At x=1.69m

Figure 5.17: Comparison of velocity profile at different cross-sections, $Q=30$

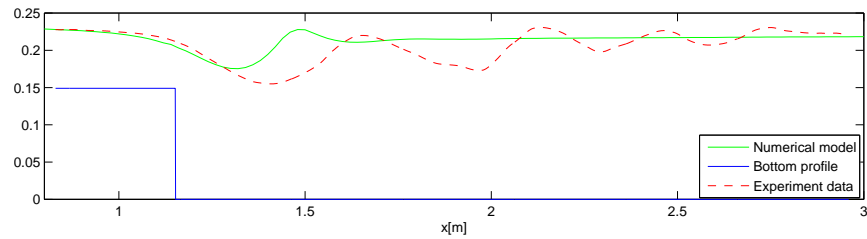


Figure 5.18: The comparison of the water profiles of numerical model with experiments data, $Q=30$ [l/s], using $k - \varepsilon$ model.

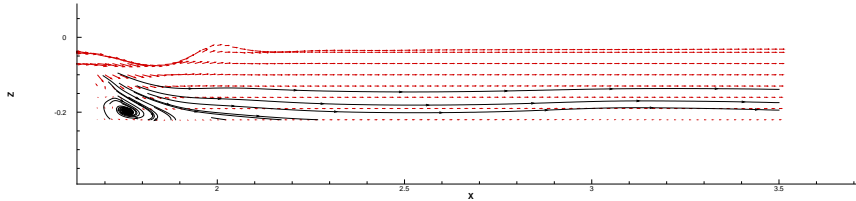


Figure 5.19: Velocity vectors behind the weir, $Q=30[l/s]$., using $k - \varepsilon$ model.

5.6 Conclusions

Details are given of the development of a two-dimensional vertical numerical model for simulating unsteady free-surface flows, using a non-hydrostatic pressure distribution. The numerical method, in which non-hydrostatic pressures and water levels are used as unknowns, couples both the local continuity equation and integrated continuity equation into the system. In doing so, the mass is locally and globally conserved. This model is proved to fairly accurately represent discontinuities in bottom topography and water surface profiles. The numerical model also has the ability to describe different flow regimes downstream of a weir, namely free flow, undulation, and fully submerged flow. This case has particular characteristics, which restrict the application of existing numerical methods:

- Abrupt changes of bottom topography.
- The pressure downstream of the weir is non-hydrostatic. The hydrostatic assumption fails to represent the flow.
- The formation of undulation downstream of the weir.
- The formation of the recirculation zones.
- The ability to capture the change of flow type in different flow conditions.

The results from the numerical model show a fair agreement with the experimental data. The standard $k - \varepsilon$ turbulence closure model fails in predicting the wave length and wave height of undulations. The turbulence model needs to be improved further.

Chapter 6

Conclusions and Recommendations

6.1 Conclusions

In this report, the water flow over a non-flat bottom has been modeled, using various numerical models, such as 1-D model, 2DV hydrostatic model, 2DV non-hydrostatic model. A implicit non-hydrostatic model is developed to solve the Navier-Stokes equation. This method approximates the non-hydrostatic vertical pressures at different vertical cell surfaces simultaneously and can guarantee local and global mass conservation. The properties and applicability of the numerical algorithms implemented in this report may be summarized as follows:

- The conservation of properties is crucial in dealing with discontinuous bed profiles and steep gradients in water levels (hydraulic jump).
- When dealing with uneven bottom profiles, the z -coordinate is not a good choice. You should take care of all the bloody tiny details to ensure that all the discretization are properly implemented.
- When solving the Shallow Water Equation with hydrostatic assumption, if the viscosity is not taken into account, the model should give identical horizontal velocities along the vertical columns.
- The non-hydrostatic model is better than the hydrostatic model.
- The implicit non-hydrostatic method allows the simulation of mixed flow (supercritical, subcritical and trans-critical flows as well as the discontinuities such as hydraulic jump. The model is capable to describe the transition from one flow pattern to another.
- By means of the 2DV non-hydrostatic model, the position of the hydraulic jump and the surface roller can be fairly well predicted.

For the simulation of undulation, the length and height of first wave is in good agreement with experimental data. This model can be used as a tool for designing hydraulic structures. Knowledge of the characteristics and the formation of undular hydraulic jumps is important for the design and maintenance of canals.

6.2 Recommendations

The 2DV hydrodynamic model has been verified by comparing model results to either analytical solutions or experimental data, for oscillating basin and hydraulic jump over a weir. It requires further testing. The following suggestions for further research are given:

- When solve the problem with abrupt changed bottom or steep water level gradient, without density current, we suggest to use sigma coordinate. Under σ -coordinate, the continuity equation at the bottom and the kinematic boundary condition at the water surface are much easier to be implemented than that of under z -coordinate.
- The turbulence closure model, namely the standard $k - \varepsilon$ model does not properly simulate the undular hydraulic jump. Better turbulence closure model is needed.
- In the implicit non-hydrostatic model, no-slip boundary condition is implemented at the bottom, i.e., $w = 0$ at the bottom. This can be improved by implementing the kinematics boundary at the bottom.
- To couple the water level into the system, beside the integrated continuity equation, the kinematic free surface boundary equation can be solved simultaneously with the Reynolds equations. The results of these two options could be compared.

Bibliography

- [1] B.A. Wols. Undular hydraulic jump. Master's thesis, TUDelft, 2005.
- [2] Casulli V, Stelling G.S. Numerical simulation of 3d quasi-hydrostatic, free-surface flows. *Journal of Hydraulic Engineering, ASCE*, 124:678–686, 1998.
- [3] Chow, V.T. *Open channel hydraulics*. New Yor, USA: McGraw-Hill International, 1973.
- [4] Harlow FH, Welch JE. Numerical calculation of time-dependent viscous incompressible flow. *Physics of Fluids*.
- [5] Hirsch C. *Numerical Computation of Internal and External Flows*. Wiley: New York, 1990.
- [6] Kolkman, P.A. Discharge relatons for hydraulic structures and head losses from different components. Technical Report A965-C67, 1989.
- [7] Rodi, W. *Turoulence Models and Their Application in Hydraulics*. IAHR Publication, 1984.
- [8] Stansby PK, Zhou JG. Shallow-water flow solver with non-hydrostatic pressure:2d vertical plane problems. *International Journal for Numerical Methods in Fluids*, 28:541–563, 1998.
- [9] Stelling, G.S. *On the construction of computational methods for shallow water flow problems*. Rijkswatertat Communication, 1984(35).
- [10] Stelling, G.S. and J.A.Th.M. Van Kester. A new vertical approximation for the numerical simulation of non-hydrostatic free surface flows. Technical report.
- [11] Stelling, G.S. and M.Zijlema. An accurate and efficient finite-difference algorithm for non-hydrostatic free-surface flow with application to wave propagation. *Internation Journal for Numerical Methods in Fluids*, 43:1–23, 2003.

- [12] Stelling, G.S. and S.P.A.Duinmeijer. A staggered conservative scheme for every froude number in rapidly varied shallow water flows. *Internation Journal for Numerical Methods in Fluids*, 43:1329–1354, 2003.
- [13] Stelling, G.S. and Busnelli, M.M. Numerical simulation of the vertical structure of discontinuous flows. *International Journal of Numerical Methods in Fluids*, 37:23–43, 2001.
- [14] M. van Reeuwijk. Efficient simulation of non-hydrostatic free-surface flow. M.sc thesis, Delft University of Technology, Faculty of Civil Engineering and Geosciences, Section Fluid Mechanics, 2002.
- [15] Zijlema, M. Computing non-hydrostatic free-surface flows with triwaq using a pressure correction technique. Technical Report Werdocument RIKZ.OS/2000, 137X, Nautilus, Rijkswater staaat.RIKZ, 2000.

with:

$$\begin{aligned}\beta_1 &= b_1 \\ \alpha_i &= \frac{a_i}{\beta_{i-1}}, \quad i = 2, 3, \dots, N \\ \beta_i &= b_i - \alpha_i c_{i-1}, \quad i = 2, 3, \dots, N\end{aligned}$$

The solution of $AV = D$ is obtained by forward elimination and backward substitution: First a vector Y is computed by $LY = D$, then the final vector V by $UV = Y$. This decomposition has the advantage that triangular matrices are easily inverted. When applied to a gridiagonal matrix, the method is applied according to the following algorithm.

$$\begin{aligned}\delta_1 &= d_1 & \delta_i &= d_i - \alpha_i \delta_{i-1}, \quad i = 2, 3, \dots, N \\ x_N &= \frac{\delta_N}{\beta_N}, & x_i &= \frac{\delta_i - c_i x_{i+1}}{\beta_i}, \quad i = N-1, N-2, \dots, 1\end{aligned}$$

The double sweep algorithm, also called Thomas algorithm is particularly economical; it requires only $5N-4$ operations (multiplications and divisions). But to prevent ill-conditioning (and hence round-off contamination) it is necessary that

$$|b_i| > |a_i| + |c_i|$$

Appendix B

Discretization of Advection terms

Advection terms in x direction

The continuity and the momentum equations, neglecting the viscosity terms and the hydrodynamic pressures, are:

$$\frac{\partial u}{\partial x} + \frac{\partial w}{\partial z} = 0 \quad (\text{B.1})$$

$$u \frac{\partial u}{\partial t} + u \frac{\partial u}{\partial x} + w \frac{\partial u}{\partial z} + g \frac{\partial \zeta}{\partial x} = 0 \quad (\text{B.2})$$

Horizontal advection

If $\bar{u}_m > \bar{u}_{m-1}$,

$$u \frac{\partial u}{\partial x} = \frac{1}{2} (u_{m,k}^n + u_{m-1,k}^n) \left(\frac{u_{m,k}^n - u_{m-1,k}^n}{\Delta x} \right) \quad (\text{B.3})$$

else if $u_{m,k}^n > 0$

$$u \frac{\partial u}{\partial x} = u_{m,k}^n \left(\frac{u_{m,k}^n - u_{m-1,k}^n}{\Delta x} \right) \quad (\text{B.4})$$

else

$$u \frac{\partial u}{\partial x} = u_{m,k}^n \left(\frac{u_{m+1,k}^n - u_{m,k}^n}{\Delta x} \right) \quad (\text{B.5})$$

Vertical advection

$$\bar{w}_+ > 0 \cap \bar{w}_- > 0$$

$$w \frac{\partial u}{\partial x} = \bar{w}_- \left(\frac{u_{m,k}^n - u_{m,k-1}^n}{\Delta z} \right)$$

$$\bar{w}_+ < 0 \cap \bar{w}_- < 0$$

$$w \frac{\partial u}{\partial x} = \bar{w}_+ \left(\frac{u_{m,k+1}^n - u_{m,k}^n}{\Delta z} \right)$$

$$\bar{w}_+ < 0 \cap \bar{w}_- > 0$$

$$w \frac{\partial u}{\partial x} = \bar{w}_+ \left(\frac{u_{m,k+1}^n - u_{m,k}^n}{\Delta z} \right) + \bar{w}_- \left(\frac{u_{m,k}^n - u_{m,k-1}^n}{\Delta z} \right)$$

(B.6)

where $\bar{w}_+ = \frac{w_{m,k}^n + w_{m+1,k}^n}{2}$, $\bar{w}_- = \frac{w_{m,k}^n + w_{m-1,k}^n}{2}$

Advection terms in z direction

The continuity and the momentum equations, neglecting the viscosity terms and hydrodynamic pressures, are:

$$\frac{\partial u}{\partial x} + \frac{\partial w}{\partial z} = 0 \quad (\text{B.7})$$

$$\frac{\partial w}{\partial t} + u \frac{\partial w}{\partial x} + w \frac{\partial w}{\partial z} = 0 \quad (\text{B.8})$$

Horizontal advection

$$\begin{aligned} \bar{u}_+ > 0 \cap \bar{u}_- > 0 & \quad u \frac{\partial w}{\partial x} = \bar{u}_- \left(\frac{w_{m,k}^n - w_{m-1,k}^n}{\Delta x} \right) \\ \bar{u}_+ < 0 \cap \bar{u}_- < 0 & \quad u \frac{\partial w}{\partial x} = \bar{u}_+ \left(\frac{w_{m+1,k}^n - w_{m,k}^n}{\Delta z} \right) \\ \bar{u}_+ < 0 \cap \bar{u}_- > 0 & \quad u \frac{\partial w}{\partial x} = \bar{u}_+ \left(\frac{w_{m+1,k}^n - w_{m,k}^n}{\Delta z} \right) + \bar{u}_- \left(\frac{w_{m,k}^n - w_{m-1,k}^n}{\Delta x} \right) \end{aligned} \quad (\text{B.9})$$

where $\bar{u}_+ = \frac{u_{m,k}^n + u_{m+1,k}^n}{2}$, $\bar{u}_- = \frac{u_{m,k}^n + u_{m-1,k}^n}{2}$

Vertical advection

$$\begin{aligned} \bar{w}_+ > 0 \cap \bar{w}_- > 0 & \quad w \frac{\partial w}{\partial x} = \bar{w}_- \left(\frac{w_{m,k}^n - w_{m,k-1}^n}{\Delta z} \right) \\ \bar{w}_+ < 0 \cap \bar{w}_- < 0 & \quad w \frac{\partial w}{\partial x} = \bar{w}_+ \left(\frac{w_{m,k+1}^n - w_{m,k}^n}{\Delta z} \right) \\ \bar{w}_+ < 0 \cap \bar{w}_- > 0 & \quad w \frac{\partial w}{\partial x} = \bar{w}_+ \left(\frac{w_{m,k+1}^n - w_{m,k}^n}{\Delta z} \right) + \bar{w}_- \left(\frac{w_{m,k}^n - w_{m,k-1}^n}{\Delta z} \right) \end{aligned} \quad (\text{B.10})$$

where $\bar{w}_+ = \frac{w_{m,k}^n + w_{m,k+1}^n}{2}$, $\bar{w}_- = \frac{w_{m,k}^n + w_{m,k-1}^n}{2}$

Appendix C

Comparison between Compact and Keller-box method

For the discretization of vertical momentum equation, there are two methods, a) Keller-box method, b) Compact method. First, we ignore the advection and viscosity terms. The vertical momentum equation becomes:

$$\frac{\partial w}{\partial t} = -\frac{\partial q}{\partial z} \quad (\text{C.1})$$

The Keller-box method discretize both the time derivative and the pressure gradient as the average of values at locations (m, k) and $(m, k - 1)$.

$$\frac{w_{m,k}^{n+1} - w_{m,k}^n + w_{m,k-1}^{n+1} - w_{m,k-1}^n}{2\Delta t} = -\frac{q_{m,k}^{n+1} - q_{m,k-1}^{n+1}}{\Delta z_{m,k}} \quad (\text{C.2})$$

$$\frac{w_{m,k}^{n+1} - w_{m,k}^n + w_{m,k-1}^{n+1} - w_{m,k-1}^n}{2\Delta t} = -\left(\frac{1}{2} \frac{\partial q}{\partial z} \Big|_{m,k} + \frac{1}{2} \frac{\partial q}{\partial z} \Big|_{m,k-1} \right) \quad (\text{C.3})$$

Eqn. (C.2) and (C.3) are the same, because we have following relation:

$$\frac{q_{m,k}^{n+1} - q_{m,k-1}^{n+1}}{\Delta z_{m,k}} = \frac{1}{2} \frac{\partial q}{\partial z} \Big|_{m,k} + \frac{1}{2} \frac{\partial q}{\partial z} \Big|_{m,k-1} \quad (\text{C.4})$$

The Compact method only discretize the time derivative and the pressure gradient at location (m, k) .

$$\frac{w_{m,k}^{n+1} - w_{m,k}^n}{\Delta t} = \frac{\partial q}{\partial z} \Big|_{m,k} \quad (\text{C.5})$$

If we add the discretization with compact method at location (m, k) and

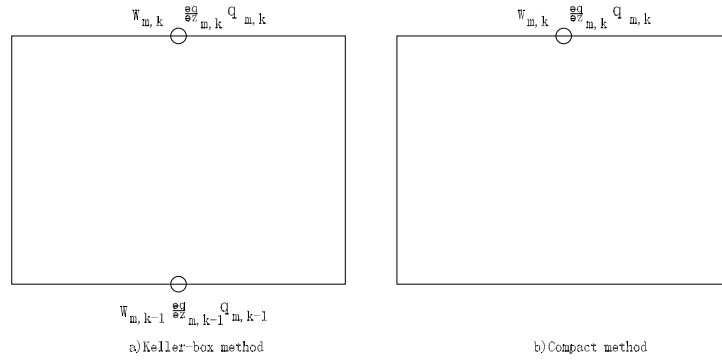


Figure C.1: The Keller-box method and Compact method

$(m, k - 1)$ up, we get the expression of Keller-box scheme. This means that if we only consider the form of $\frac{\partial w}{\partial t} = -\frac{\partial q}{\partial z}$, there is no difference between the Keller-box and compact method. So the only difference between these two methods just depend upon how we discretize the advection and viscosity terms. However, during the programming, we found, after taking the advection and viscosity terms into account, sometimes the Keller-box scheme became ill-posed. The final system matrix is singular. Another drawback of Keller-box method is, when discretize the vertical viscosity term, we have to introduce $\frac{\partial w}{\partial z}$ as additional unknown, which makes the programming work more complicated.